

Electrotrophy as potential primary metabolism for colonization of conductive surfaces in deep-sea hydrothermal chimneys

Guillaume Pillot, Sylvain Davidson, Laetitia Shintu, Oulfat Amin, Anne Godfroy, Yannick Combet-Blanc, Patricia Bonin, Pierre-Pol Liebgott

▶ **To cite this version:**

Guillaume Pillot, Sylvain Davidson, Laetitia Shintu, Oulfat Amin, Anne Godfroy, et al.. Electrotrophy as potential primary metabolism for colonization of conductive surfaces in deep-sea hydrothermal chimneys. 2020. hal-03022667

HAL Id: hal-03022667

https://amu.hal.science/hal-03022667

Preprint submitted on 24 Nov 2020

HAL is a multi-disciplinary open access archive for the deposit and dissemination of scientific research documents, whether they are published or not. The documents may come from teaching and research institutions in France or abroad, or from public or private research centers.

L'archive ouverte pluridisciplinaire **HAL**, est destinée au dépôt et à la diffusion de documents scientifiques de niveau recherche, publiés ou non, émanant des établissements d'enseignement et de recherche français ou étrangers, des laboratoires publics ou privés.

bioRxiv preprint doi: https://doi.org/10.1101/2020.11.11.377697; this version posted November 11, 2020. The copyright holder for this preprint (which was not certified by peer review) is the author/funder. All rights reserved. No reuse allowed without permission.

Electrotrophy as potential primary metabolism for colonization of conductive surfaces in deep-sea hydrothermal chimneys.

Guillaume Pillot[1], Sylvain Davidson[1], Laetitia Shintu[3], Oulfat Amin Ali[X], Anne Godfroy[2], Yannick Combet-Blanc[1], Patricia Bonin[1], Pierre-Pol Liebgott[1*]

[1] Aix Marseille Univ., Université de Toulon, IRD, CNRS, MIO UM 110, 13288, Marseille, France

[2] IFREMER, CNRS, Université de Bretagne Occidentale, Laboratoire de Microbiologie des Environnements Extrêmes – UMR6197, Ifremer, Centre de Brest CS10070, Plouzané, France.

[3]Aix Marseille Univ, CNRS, Centrale Marseille, iSm2, Marseille, France

[*] To whom correspondence may be addressed. Email: pierre-pol.liebgott@mio.osupytheas.fr; Mediterranean Institute of Oceanography, Campus de Luminy, Bâtiment OCEANOMED, 13288 Marseille Cedex 09.

https://orcid.org/0000-0002-2559-1738

Key-words

Electrotrophy, hyperthermophiles, microbial electrochemical system, deep-sea hydrothermal vent, electrosynthesis

Summary

Deep-sea hydrothermal vents are extreme and complex ecosystems based on a trophic chain. We are still unsure of the first colonizers of these environments and their metabolism, but they are thought to be (hyper)thermophilic autotrophs. Here we investigate whether the electric potential observed across hydrothermal chimneys could serve as an energy source for these first colonizers. Experiments were performed in a two-chamber microbial electrochemical system inoculated with deep-sea hydrothermal chimney samples, with a cathode as sole electron donor, CO_2 as sole carbon source, and three different electron acceptors (nitrate, sulfate, and oxygen). After a few days of culture, all three experiments showed growth of an electrotrophic biofilm consuming directly or indirectly the electrons and producing organic compounds including acetate, glycerol,

bioRxiv preprint doi: https://doi.org/10.1101/2020.11.11.377697; this version posted November 11, 2020. The copyright holder for this preprint (which was not certified by peer review) is the author/funder. All rights reserved. No reuse allowed without permission.

and pyruvate. The only autotrophs retrieved were members of *Archaeoglobales*, in all three experiments. Various heterotrophic phyla also grew through trophic interactions, with *Thermococcales* in all three experiments and other bacterial groups specific to each electron acceptor. This electrotrophic metabolism as energy source to drive the first microbial colonization of conductive hydrothermal chimneys was discussed.

Introduction

Deep-Sea hydrothermal vents, are geochemical structures housing an extreme ecosystem rich in micro- and macro-organisms. Since their discovery in 1977 (Corliss and Ballard, 1977), they attracted the interest of researcher and, more recently, industries by their singularities. Isolated in the deep ocean, far from the sunlight and subsequent organic substrate, the primal energy sources for the development of this luxuriant biosphere remain elusive in these extreme environments rich in minerals. Since their discovery, many new metabolisms have been identified based on organic or inorganic molecules. However, the driving force sustaining all biodiversity in these environments is thought to be based on chemolithoautotrophy (Alain *et al.*, 2004). Indeed, unlike most ecosystems, deep-sea ecosystems are totally dark and microorganisms have adapted to base their metabolism on lithoautotrophy using inorganic compounds as the energy source to fix inorganic carbon sources. Primary colonizers of deep-sea hydrothermal vents are assumed to be (hyper)thermophilic microbes developing near the hydrothermal fluid, as retrieved in young hydrothermal chimneys. These first colonizers are affiliated to *Archaea*, such as *Archaeoglobales*, *Thermococcales*, *Methanococcales* or *Desulfurococcales*, and to *Bacteria* from ε-*proteobacteria* and *Aquificales*. (Huber *et al.*, 2002, 2003; Nercessian *et al.*, 2003; Takai *et al.*, 2004). Recent studies have also shown that hyperthermophilic *Archaea*, which count among the supposed first colonizers, are able to quickly scan and fix onto surfaces to find the best conditions for growth (Wirth *et al.*, 2018). These hyperthermophilic microorganisms would fix inorganic carbon through

bioRxiv preprint doi: https://doi.org/10.1101/2020.11.11.377697; this version posted November 11, 2020. The copyright holder for this preprint (which was not certified by peer review) is the author/funder. All rights reserved. No reuse allowed without permission.

chemolithoautotrophic types of metabolism, using H_2, H_2S or CH_4 as energy sources and oxidized molecules such as oxygen, sulfur compounds, iron oxide or even nitrate as electron acceptors.

However, the discovery of the presence of an abiotic electric current across the chimney walls (Yamamoto *et al.*, 2017) prompted the hypothesis of a new type of microorganisms called eletrotrophs having the capacity to use electrons from the abiotic electric current as an energy source coupled with carbon fixation from CO_2. This metabolism was identified a few years ago on a mesophilic chemolithoautotrophic Fe(II)-oxidizing bacterium, *Acidithiobacillus ferrooxidans* (Ishii *et al.*, 2015). This strain was able to switch its source of energy from diffusible Fe^{2+} ions to direct electron uptake from a polarized electrode. However, this feature has not yet been demonstrated in deep-sea hydrothermal vent environments. Recent studies have shown the exoelectrogenic ability of some hyperthermophilic microorganisms isolated from deep-sea hydrothermal vents, belonging to *Archaeoglobales* and *Thermococcales* (Pillot *et al.*, 2018, 2019; Yilmazel *et al.*, 2018), but no studies have been done on environmental samples potentially harboring electrotrophic communities growing naturally with an electric current as sole energy source.

Here, we investigate the potential presence of electrotrophic communities in deep-sea hydrothermal vents capable of using electrons directly or indirectly from the abiotic current. In this purpose, we mimic the conductive surface of the hydrothermal chimney in a cathodic chamber of Microbial Electrochemical Systems (MES) with a polarized cathode to enrich the potential electrotrophic communities inhabiting these extreme environments. The polarized cathode served as the sole energy source, while CO_2 bubbling served as sole carbon source. Three electron acceptors were tested separately, i.e. nitrate, oxygen, and sulfate, to show the influence of an electron acceptor on community taxonomic composition.

Results

Current consumption from electrotroph enrichments

bioRxiv preprint doi: https://doi.org/10.1101/2020.11.11.377697; this version posted November 11, 2020. The copyright holder for this preprint (which was not certified by peer review) is the author/funder. All rights reserved. No reuse allowed without permission.

Hydrothermal vents chimney samples were inoculated in MES filled with sterile mineral medium and incubated at 80°C to enrich electrotrophic communities. In the latter, the electrode served as the sole energy donor (cathode) and sparged CO_2 as carbon source with three different electron acceptors that were tested separately: (i) nitrate, (ii) sulfate and (iii) oxygen. The microbial electrotrophic enrichment was monitored at lowest possible potentials. These potentials were poised at -300mV/SHE in presence of oxygen and -590mV/SHE for both nitrate and sulfate, respectively. For comparison, microbial growth was also monitored without any poised potential during a month in the same conditions of incubation. Interestingly, in the latter condition, no microbial growth occurred, supported by microscope and spectrophotometric observations (data not shown). Moreover, no organic compounds were produced supported by the HPLC and NMR measurements (data not shown).

When potential was poised, abiotic controls containing no inoculum displayed constant currents of ≈0,016 $A.m^{-2}$ at -590 mV and ≈0,01 $A.m^{-2}$ at -300 mV/SHE. In both conditions, the potential hydrogen production on the cathode by water electrolysis was quantified and was under the detection threshold of the µGC (>0.001% of total gas), indicating a theoretical production lower than 34 µM day-1 (data not shown), similar as previously reported at 25°C (Marshall *et al.*, 2013). In comparison, experiments with the chimney sample showed current consumptions increasing shortly after inoculation (Fig. 1). Indeed, when subtracting abiotic current, the current consumptions reached a stabilized maximum of 0.36 $A.m^{-2}$ on oxygen, 0.72 $A.m^{-2}$ on nitrate, and up to 1.83 $A.m^{-2}$ on sulfate corresponding therefore to an increase of 36, 45 and 114-fold compared to abiotic current, respectively. MES were autoclaved afterwards displaying decreased currents that were similar to the values of abiotic controls with a stabilized current around ≈0,021 $A.m^{-2}$.

At the end of monitoring of current consumption, CycloVoltamograms (CV) were performed to study reactions of oxidation and reduction that could occur in MES (Supporting Information Fig.

bioRxiv preprint doi: https://doi.org/10.1101/2020.11.11.377697; this version posted November 11, 2020. The copyright holder for this preprint (which was not certified by peer review) is the author/funder. All rights reserved. No reuse allowed without permission.

S1A). A first peak of reduction is observed at -0.295, -0.293 and -0.217 V vs SHE in presence of nitrate, sulfate and oxygen as electron acceptor, respectively (Fig. S1B). A second peak is observed at -0.639 and -0.502 V vs SHE on nitrate and sulfate, respectively. No redox peaks are detected in the abiotic controls and freshly inoculated MES, hence indicating a lack of electron shuttles brought with the inoculum (Fig. S1A).

Organic compounds production in liquid media

During enrichment of the electrotrophic communities, the production of organic compounds was monitored in liquid media (Fig. 1). Interestingly, the glycerol, the pyruvate, and the acetate were the dominant products released in all experiment runs. Glycerol increased slowly throughout the experiments to reach a maximum of 0.47 mM on sulfate (day 11), 1.32 mM on oxygen (day 12) and 2.32 mM on nitrate (day 19). Acetate accumulated in the medium to reach 0.33 mM on oxygen (day 7), 0.75 mM on sulfate (day 13) and 1.40 mM on nitrate (day 19). Pyruvate was produced after a few days of culture with an exponential curve, reaching a maximum of 1.32 mM on oxygen (day 12), 2.39 mM on nitrate (day 9), and 3.94 mM on sulfate (day 11). Pyruvate varied, afterwards, due probably to microbial consumption or thermal degradation... Coulombic efficiency calculated on the last day of the experiment (Fig. 2) showed up to 71% (on nitrate), 89% (on oxygen) and 90% (on sulfate) of electrons consumed were converted to organic compounds and released into the liquid media .The rest represents the share of electrons retained in not accumulated compounds (Table S1) and in the organic matter constituting the cells of the electrotrophic communities (estimated by qPCR to total between 10^8 to 10^{10} 16S rRNA gene copies per MES; Supporting Information Fig. S2).

Biodiversity of electrotrophic communities on different electron acceptors

Once current consumption reached a stabilized maximum, DNAs from the biofilm and from planktonic cells in culture media were extracted and sequenced on the V4 region of the 16S rRNA

bioRxiv preprint doi: https://doi.org/10.1101/2020.11.11.377697; this version posted November 11, 2020. The copyright holder for this preprint (which was not certified by peer review) is the author/funder. All rights reserved. No reuse allowed without permission.

to study relative abundance of the biodiversity. Fig. 3 reports the taxonomic affiliation of the OTUs obtained. The chimney fragment inoculum showed a rich biodiversity (Shannon index at 5.29 and Pielou's index at 0.69), with 208 OTUs mainly affiliated to *Bacteria* (99.49% *vs* 0.51% of *Archaea*) and more particularly to *Proteobacteria* from *Vibrionales* (34.8%), miscellaneous rare *Proteobacteria* (>33%), *Campylobacterales* (8.3%), *Thermales* (7.1%), *Aquificales* (5.62%), and *Rhodobacterales* (5.1%) .

Enrichments in MES showed less biodiversity on cathodes and liquid media, suggesting the selective development of functional communities. The Shannon index values were 3.1 and 1.9 on nitrate, 1.7 and 1.9 on sulfate, and 4.1 and 4.2 on oxygen, with fewer OTUs associated to 72 and 68 OTUs on nitrate, 39 and 53 on sulfate, and 94 and 102 on oxygen, on electrodes and liquid media, respectively. The taxonomic composition of these communities showed a larger proportion of *Archaea*, with 51% and 41.6% on nitrate, 96.8% and 96.3% on sulfate, and 7.6% and 3.4% on oxygen on the electrodes and liquid media, respectively. In presence of each electron acceptor, the archaeal population on the electrode was mainly composed of *Archaeoglobales* and *Thermococcales* at different relative abundances. The latter were present at 6.7% and 28.2% on nitrate to 65.8% and 28.6% on sulfate and 3.8% and 3.6% on oxygen, respectively. Equivalent proportions of *Archaeoglobales* and *Thermococcales* were retrieved in liquid media, at 1.0% and 2.5% on nitrate, 65.8% and 29.6% on sulfate and 0.3% and 2.7% on oxygen, respectively (Fig. 3). The MiSeq Illumina results served to study only 290 bp of 16S rRNA and thus to affiliate microorganisms confirmed at family level, but they can also provide some information on the enriched genera. In an effort to obtain more information on the probable *Archaeoglobales* and *Thermococcales* genus, we attempted a species-level identification through phylogenetic analysis. The results are presented in Fig. 4 as a Maximum Likelihood phylogenetic tree. The dominant OTUs on sulfate and oxygen were closest to *Ferroglobus placidus* and *Archeoglobus fulgidus* 97.61% whereas the dominant OTU on nitrate was affiliated to *Geoglobus ahangari* with an

bioRxiv preprint doi: https://doi.org/10.1101/2020.11.11.377697; this version posted November 11, 2020. The copyright holder for this preprint (which was not certified by peer review) is the author/funder. All rights reserved. No reuse allowed without permission.

identity of 98.63% of identity. The remaining part of the biodiversity was specific to each electron acceptor used. Enrichment on nitrate showed 13.8% and 28% of *Desulfurococcales* and 46.2% and 56.5% of *Thermales* on the electrode and in liquid media, respectively. Among *Thermales* that developed on the electrode, 30% were represented by a new taxon (OTU 14 in Fig. 4 and S3) whose closest cultured species was *Vulcanithermus mediatlanticus* (90% similarity). On sulfate, the remaining biodiversity represented less than 4% of the population but was mainly represented by two particular OTUs. The first OTU, accounting for up to 2.4% and 0.8% of the total population on the electrode and liquid media, respectively, was affiliated to a new *Euryarchaeota* (OTU 10 in Fig. 4 and S3) whose closest cultured match was *Methanothermus fervidus* strain DSM 2088, at 86% similarity. The second OTU accounted for 2.0% and 1.9% of the biodiversity on the electrode and liquid media, respectively, and was affiliated to the new *Deinococcales* (OTU 14 in Fig. 4 and S3) species, found mostly on the electrode in nitrate enrichment. In the enrichment on oxygen, the communities are dominated by 36.6% and 30.2% of *Pseudomonadales* (Pseudomonas sp.), 14% and 42.6% of *Bacillales* (*Bacillus* and *Geobacillus* sp.), 21.3% and 7.41% of *Vibrionales* (*Photobacterium* sp.), and 9.8% and 5.1% of *Actinomycetales* (spread across 9 species) on the electrode and in liquid media, respectively, with the rest spread across *Proteobacteria* orders.

The clustering of the dominant OTUs (at a threshold of 0.05% of total sequences) obtained previously on the chimney sample and enrichments in MES showed a clear differentiation of communities retrieved in each sample (Supporting Information Fig. S3). The Pearson method on OTU distribution produced four clusters, one corresponding to the inoculum and the three others to each electron acceptor. Indeed, only two OTUs (OTU 4 and 36) were clearly shared between two different communities, one affiliated to *Thermococcus* spp. on nitrate and sulfate and one to *Ralstonia* sp. on the chimney sample and on nitrate. It is surprising to observe a recurrence of this last OTU which could be a contaminant specific to the extraction kit used (Salter *et al.*, 2014). The

bioRxiv preprint doi: https://doi.org/10.1101/2020.11.11.377697; this version posted November 11, 2020. The copyright holder for this preprint (which was not certified by peer review) is the author/funder. All rights reserved. No reuse allowed without permission.

other 50 dominant OTUs were specific to one community, with 21 OTUs on oxygen, 4 on sulfate, 8 on nitrate, and 17 on the chimney sample. The electrotrophic communities, colonizing the cathode, were therefore different depending on electron acceptor used and their concentration was too low to be detected in the chimney sample.

Discussion

Archaeoglobales as systematic (electro)lithoautotrophs of the community

Herein, we evidenced the development of a microbial electrotrophic communities and metabolic activity supported by current consumption (Fig.1), product production (Fig. 2), and qPCRs (Fig. S2) suggesting that growth did occur from energy supplied by the cathode. The mechanism of energy uptake from electrode is discussed since the discovery of biofilms growing on cathode, and little is known, unlike electron transfer mechanism on anode. The two main hypotheses are the use of similar direct electron transfer pathway as on the anode, or the use of molecular H_2, produced by water electrolysis, as electron mediator to the cell. In both cases, our study is the first to show the possibility of growth of biofilm from environments harboring natural electric current in absence of organic substrates. To discuss further on the putative mechanism, it is necessary to have a look on the conditions for water electrolysis. The potential for water reduction into hydrogen at 80°C, ph7, 1 atm was calculated at −0.490 V vs SHE in pure water. The real operational reduction potentials is expected to be much more lower than the theoretical value due to internal resistances (from electrical connections, electrolyte, ionic membrane etc.) (Lim *et al.*, 2017). Moreover, overpotentials are expected with carbon electrodes. The decrease of this potential explains the absence of hydrogen measured in our conditions. A screening of potential in abiotic conditions confirmed the increase of current consumption and H_2 production only at potential lower of -0.6V vs SHE (Fig S1) Moreover several pieces of evidence indicate that direct electron transfer may have mainly participated in the development of biofilms: the growth of the similar dependent sulfate biodiversity with the cathode poised at -300 mV vs SHE (Supporting Information Fig. S4) without H_2

bioRxiv preprint doi: https://doi.org/10.1101/2020.11.11.377697; this version posted November 11, 2020. The copyright holder for this preprint (which was not certified by peer review) is the author/funder. All rights reserved. No reuse allowed without permission.

198 production, the expression of catalytic waves observed by CV with midpoint potentials between -
199 0.217 V to -0.639 V and the lack of similar peaks with abiotic or fresh inoculated media (Supporting
200 Information Fig. S1), biofilm formation on the electrode (as on nitrate, Supporting Information Fig.
201 S5), delayed production of glycerol, pyruvate and acetate (Fig. 1) fixing between 267 to 1596
202 Coulombs.day^{-1} (organic consumption deduced), and the recovery of electrons in all three products
203 (Fig. 2), that largely exceeds the maximum theoretical abiotic generation of hydrogen (~3 C.day^{-1})
204 by 90 to 530-fold. Thus, we can assume that the biofilm growth was largely ensured by a significant
205 part of a direct transfer of electrons from the cathode demonstrating the presence of
206 electrolithoautotroph microorganisms.

207 Taxonomic analysis of the enriched microbial communities at the end of the experiments showed
208 the systematic presence on cathodes of *Archaeoglobales* (Fig. 3 and S3), whatever the electron
209 acceptors used. The species belonging to *Archaeoglobales* order were the only enriched species in
210 all conditions and the only known to have an autotrophic metabolism (except for *Archaeoglobus*
211 *profundus* and *A. infectus* which are obligate heterotrophs). The *Archaeoglobales* order is
212 composed of three genera: *Archaeoglobus*, *Geoglobus*, and *Ferroglobus*. All are hyperthermophilic
213 obligate anaerobes with diverse metabolisms, including heterotrophy or chemolithoautotrophy.
214 Terminal electron acceptors used by this order include sulfate, nitrate, poorly crystalline Fe (III)
215 oxide, or sulfur oxyanions (Brileya and Reysenbach, 2014). Autotrophic growth in the
216 *Archaeoglobales* order is ensured mainly through H_2 as energy source and requires both branches
217 of the reductive acetyl-CoA/Wood-Ljungdahl pathway for CO_2 fixation (Vorholt *et al.*, 1997).
218 Moreover, *Archaeoglobus fulgidus* has been recently shown to grow on iron by directly snatching
219 electrons under carbon starvation during corrosion process (Jia *et al.*, 2018). Furthermore,
220 *Ferroglobus* and *Geoglobus* species were shown to be exoelectrogens in pure culture in a microbial
221 electrosynthesis cell (Yilmazel *et al.*, 2018) and were enriched during a study within a microbial
222 electrolysis cell (Pillot *et al.*, 2018, 2019). Interestingly, some studies have shown that *Geobacter*

bioRxiv preprint doi: https://doi.org/10.1101/2020.11.11.377697; this version posted November 11, 2020. The copyright holder for this preprint (which was not certified by peer review) is the author/funder. All rights reserved. No reuse allowed without permission.

223 species are capable of bidirectional electron transfer using the same mechanism (Pous *et al.*, 2016).
224 Hence, *Archaeoglobales* that have been shown already as exoelectrogens (Yilmazel *et al.*, 2018)
225 could also be electrotrophs. It is not known how Archaea carry out exogenous electron transfer. As
226 previously discussed, the absence of H_2 production and the increasing current consumptions over
227 time suggest direct electron uptake from members of the communities developing on the
228 electrode, as for *Acidithiobacillus ferroxidans* (Ishii *et al.*, 2015). Moreover, the qPCR (Supporting
229 Information Fig. S2) and MiSeq data (Fig. 3) highlighted a strong correlation between current
230 consumption and density of *Archaeoglobales* on the electrode (R^2=0.962). In the condition with
231 sulfate as electron acceptor, the proportion of *Archaeoglobales* represented 65.8% of total
232 biodiversity providing 1.83 $A.m^{-2}$ of current consumption, compared to only 6.7% in the nitrate
233 condition and 3.8% in the oxygen condition for 0.72 and 0.36 $A.m^{-2}$ of current consumption,
234 respectively. Moreover, the majority of OTUs were affiliated to three *Archaeoglobaceae* genera,
235 mainly *Archaeoglobus* spp. and *Ferroglobus* spp. on sulfate and oxygen and *Geoglobus* sp. on
236 nitrate. Some *Archaeoglobus* are known to show anaerobic sulfate-reducing metabolism while
237 *Ferroglobus* spp. are not. *Geoglobus* sp. has never been described to perform nitrate reduction so
238 far, but it does harbor genes of nitrate- and nitrite-reductase-like proteins (Manzella *et al.*, 2015).
239 The OTUs were related to some *Archaeoglobales* strain with 95-98% identities. Thus, we assume
240 that in our conditions, new specific electrotrophic metabolisms or new electrolithoautotrophic
241 *Archaeoglobaceae* species were enriched on the cathode. Moreover, a member of a new
242 phylogenetic group of *Archaea* was enriched up to 2.4% of total biodiversity on sulfate (OTU10 in
243 Fig. 4). While its metabolism is still unknown, we suggest that isolation of this electrotrophic
244 archaea in MES could enable the identification of a new archaeal phylogenetic group based on
245 electrotrophy.

246 The growth of *Archaeolgobales* species in presence of oxygen is a surprising finding.
247 *Archaeoglobales* have a strictly anaerobic metabolism, and the reductive acetyl-CoA pathway is

bioRxiv preprint doi: https://doi.org/10.1101/2020.11.11.377697; this version posted November 11, 2020. The copyright holder for this preprint (which was not certified by peer review) is the author/funder. All rights reserved. No reuse allowed without permission.

very sensitive to the presence of oxygen (Fuchs, 2011). This can be firstly explained by the low solubility of oxygen at 80°C combined with the electrochemically oxygen reduction on electrode in controls (data not shown). It hence results in an low oxygen or oxygen-free environment within the carbon cloth mesh for anaerobic development of microorganisms into a protective biofilm (Hamilton, 1987). This observation was also supported by the near absence of *Archaeoglobales* in the liquid media (Fig. 3). In absence of other electron acceptors, some *Archaeoglobales* perform carboxydotrophic metabolism to grow from CO, as demonstrated for *Archaeoglobus fulgidus* (Sokolova and Lebedinsky, 2013; Hocking *et al.*, 2015). This fermentative CO metabolism leads to the production of acetate and transient accumulation of formate via the Wood-Ljungdahl pathway, but no net ATP is really produced (Henstra *et al.*, 2007). The energy conservation through this metabolism in *Archaeoglobus fulgidus* is still poorly understood (Hocking *et al.*, 2015). A second hypothesis concerns direct interspecies electron transfer (DIET) (Kato *et al.*, 2012; Lovley, 2017), with *Archaeoglobales* transferring electrons to another microorganism as an electron acceptor. Research into DIET is in its early stages, and further investigations are required to better understand the diversity of microorganisms and the mechanism of carbon and electron flows in anaerobic environments (Lovley, 2017) such as hydrothermal ecosystems.

Electrosynthesis of organic compounds

The pyruvate, the glycerol and the acetate accumulated, while another set of compounds that appear transiently were essentially detectable in the first few days of biofilm growth (Supporting Information Table S1). They included amino acids (threonine, alanine) and volatile fatty acids (formate, succinate, lactate, acetoacetate, 3-hydroxyisovalerate) whose concentrations did not exceed one micromole. Despite their thermostability, this transient production suggests they were used by microbial communities developing on the electrode in interaction with the primary producers during enrichment.

bioRxiv preprint doi: https://doi.org/10.1101/2020.11.11.377697; this version posted November 11, 2020. The copyright holder for this preprint (which was not certified by peer review) is the author/funder. All rights reserved. No reuse allowed without permission.

On the other hand, in presence of nitrate, sulfate and oxygen as electron acceptors, the liquid media accumulated three main organic products acetate, glycerol, and pyruvate (Fig. 1). Coulombic efficiency calculations (Fig. 2) showed that redox levels of the carbon-products represented 71%–90% of electrons consumed, and only about 10%–30% of net electrons consumed by electrotrophs during growth was used directly for biomass or transferred to an electron acceptor. This concurs with the energy yield from the Wood-Ljungdahl pathway of *Archaeoglobales*, with only 5% of carbon flux directed to the production of biomass and the other 95% diverted to the production of small organic end-products excreted from the cell (Fast and Papoutsakis, 2012).

However, the production of pyruvate and glycerol warrants further analysis. Pyruvate is normally a central intermediate of CO_2 uptake by the reducing route of the acetyl-CoA/WL pathway (Berg *et al.*, 2010). It can be used to drive the anabolic reactions needed for biosynthesis of cellular constituents. Theoretically, the only explanation for improved production and accumulation of pyruvate (up to 5 mM in the liquid media of sulfate experiment) would be that pyruvate-using enzymes were inhibited or that pyruvate influx exceeded its conversion rate. Here we could suggest that in-cell electron over-feeding at the cathode leads to significant production of pyruvate. Indeed, in a physiological context, the production of pyruvate from acetyl-CoA via pyruvate synthase requires the oxidation of reduced ferredoxins for CO_2 fixation (Furdui and Ragsdale, 2000). The continuous electron uptake from the cathode would lead to a significant reduction in electron carriers (including ferredoxins, flavins, cytochromes, and/or nicotinamides), thus forcing the electrotrophic microbial community to produce pyruvate as a redox sink.

In the same context of pyruvate production, glycerol is produced by reduction of dihydroxyacetone phosphate a glycolytic intermediate, to glycerol 3-phosphate (G3P) followed by dephosphorylation of G3P to glycerol. In some yeasts, glycerol production is essential for osmoadaptation but equally for regulating the NADH surplus during anaerobic growth (Björkqvist

bioRxiv preprint doi: https://doi.org/10.1101/2020.11.11.377697; this version posted November 11, 2020. The copyright holder for this preprint (which was not certified by peer review) is the author/funder. All rights reserved. No reuse allowed without permission.

297 *et al.*, 1997). A similar mechanism may operate in our conditions for the probable excess of NADH
298 pool due to the electrode poised at -590 mV *vs* SHE, which would explain the accumulation of
299 glycerol found in our experiments.

300 In an ecophysiological context, a similar pyruvate and glycerol production could occur on
301 hydrothermal chimney walls into which electric current propagates (Yamamoto *et al.*, 2017). The
302 electrotroph biofilms would continually receive electrons, leading to the excess of intracellular
303 reducing power that would be counterbalanced by the overproduction of glycerol and pyruvate.
304 Moreover, glycerol is an essential compound in the synthesis of membrane lipids in *Archaea* and
305 probably also in biofilm formation and osmoadaptability (Desai *et al.*, 2013; Shemesh and Chai,
306 2013). Pyruvate unites several key metabolic processes, such as its conversion into carbohydrates,
307 fatty acids or some amino acids. Furthermore, these products can serve as carbon and energy
308 sources for heterotrophic microorganisms or for fermentation. In our experiments, pyruvate and
309 glycerol concentrations varied over time, suggesting they were being consumed by heterotrophic
310 microorganisms. Acetate production would thus result from the fermentation of pyruvate or
311 other compounds produced by electrotrophic *Archaeoglobales*.

312 **Enrichment of rich heterotrophic biodiversity from electrotrophic Archaeoglobales**
313 **community**

314 During our enrichment experiments, the development of effective and specific biodiversity was
315 dependent on the electron acceptors used (Fig. 3). Heatmap analyses (Supporting Information Fig.
316 3) showed four distinct communities for the three electron acceptors and the initial inoculum. Thus,
317 at the lower taxonomic level of the biodiversity analysis, most OTUs are not shared between each
318 enrichment, except for one OTU of *Thermococcales* that was shared between the nitrate and sulfate
319 experiments. This suggests a real specificity of the communities and a specific evolution or
320 adaptation of the members of the shared phyla to the different electron acceptors available in the
321 environment. However, the various enrichments also showed the presence of *Thermococcales*

bioRxiv preprint doi: https://doi.org/10.1101/2020.11.11.377697; this version posted November 11, 2020. The copyright holder for this preprint (which was not certified by peer review) is the author/funder. All rights reserved. No reuse allowed without permission.

322 regardless of the electron acceptors used, thus demonstrating a strong interaction between
323 *Thermococcales,* heterotrophs, and *Archaeoglobales,* the only autotrophs. In a previous study,
324 enrichments on the anode of a microbial electrolysis cell showed a similar tendency, with
325 *Archaeoglobales* strongly correlated to *Thermococcales* (Pillot *et al.*, 2018, 2019). Moreover,
326 members of these two groups have frequently been found together in various hydrothermal sites
327 on the surface of the Earth (Corre *et al.*, 2001; Nercessian *et al.*, 2003; Takai *et al.*, 2004; Jaeschke
328 *et al.*, 2012), where they are considered as potential primary colonizers of their environments (33–
329 36). This could point to a co-evolution and metabolic adaptation of these microorganisms to their
330 unstable environmental conditions in hydrothermal settings. After *Thermococcales*, the rest of the
331 heterotrophic biodiversity was specific to each electron acceptor.
332 On nitrate, two additional phylogenetic groups were retrieved: *Desulfurococcales* and *Thermales*.
333 OTUs of *Desulfurococcales* are mainly affiliated to *Thermodiscus* or *Aeropyrum* species, which are
334 hyperthermophilic and heterotrophic *Crenarchaeota* growing by fermentation of complex organic
335 compounds or sulfur/oxygen reduction (Huber and Stetter, 2015).
336 Concerning *Thermales*, a new taxon was enriched on cathode and only affiliated with 90 %
337 similarity to *Vulcanithermus mediatlanticus*. On sulfate, beside the large majority of
338 *Archaeoglobales* and *Thermococcales* (up to 94%–96%), this new taxon of *Thermales* (OTU 14, Fig.
339 S3) has also been enriched on the cathode, representing 2% of total biodiversity. *Thermales* are
340 thermophilic (30°C–80°C) and heterotrophic bacteria whose only four genera (*Marinithermus*,
341 *Oceanithermus*, *Rhabdothermus*, and *Vulcanithermus*) are all retrieved in marine hydrothermal
342 systems. They are known to be aerobic or microaerophilic. Some strains grow anaerobically with
343 several inorganic electron acceptors such as nitrate, nitrite, Fe (III) and elemental sulfur
344 (Albuquerque and Costa, 2014). All of the species *Thermales* can utilize the pyruvate as carbon
345 and energy source. The produced pyruvate would be a substrate of choice for this new taxon
346 which would use the sulfate and nitrate as electron acceptors.

bioRxiv preprint doi: https://doi.org/10.1101/2020.11.11.377697; this version posted November 11, 2020. The copyright holder for this preprint (which was not certified by peer review) is the author/funder. All rights reserved. No reuse allowed without permission.

Pseudomonadales and *Bacillales* were found in the oxygen experiment. Most *Pseudomonas* are known to be aerobic and mesophilic bacteria, with a few thermophilic species, including the autotrophic *Pseudomonas thermocarboxydovorans* that grows at up to 65°C (Lyons *et al.*, 1984; Palleroni, 2015). There have already been reports of mesophilic *Pseudomonas* species growing in thermophilic conditions in composting environments (Droffner *et al.*, 1995). Moreover, some *Pseudomonas* sp. are known to be electroactive in microbial fuel cells, through long-distance extracellular electron transport (Shen *et al.*, 2014; Maruthupandy *et al.*, 2015; Lai *et al.*, 2016), and were dominant on the cathodes of a benthic microbial fuel cell on a deep-ocean cold seep (Reimers *et al.*, 2006). In *Bacillales*, the *Geobacillus* spp. and some *Bacillus* sp. are known to be mainly (hyper)thermophilic aerobic and heterotrophic *Firmicutes* (Vos, 2015).

Hydrothermal electric current: a new energy source for the development of primary producers

The presence of so many heterotrophs in an initially autotrophic condition points to the hypothesis of a trophic relationship inside the electrotrophic community (Fig. 5). This suggests that the only autotrophs retrieved in all communities, the *Archaeoglobales,* might be the first colonizer of the electrode, using CO_2 as carbon source and cathode as energy source. Studies have shown how modeling and field observations can be usefully combined to describe the relationship between chemical energy conditions and metabolic interactions within microbial communities (Lin *et al.*, 2016; Dahle *et al.*, 2018). However, the models predicted low abundances of *Archaeoglobales* (<0.04%) whereas on-field detection found abundances of more than 40% in the inner section of the studied hydrothermal chimney (Dahle *et al.*, 2018). Indeed, in these models, the predicted H_2 concentration, based on observations, would be too low to support the growth of hydrogenotrophic or methanogenic species (Lin *et al.*, 2016). The authors concluded on a probable H_2 syntrophy, with hydrogen being produced by heterotrophic microorganisms such as fermentative *Thermococcales* species. Our study is the first evidence of the development of

bioRxiv preprint doi: https://doi.org/10.1101/2020.11.11.377697; this version posted November 11, 2020. The copyright holder for this preprint (which was not certified by peer review) is the author/funder. All rights reserved. No reuse allowed without permission.

hyperthermophilic electrotrophic/heterotrophic communities directly enriched from the natural environment known to harbor natural electric current as a potential energy source. We can thus conclude that this kind of electrolithoautotrophic metabolism is highly likely in deep-sea hydrothermal ecosystems, which raises the question of the importance of this metabolism in the primary colonization of hydrothermal vents. The hydrothermal electric current could make up for the lack of H_2 normally needed to sustain the growth of hydrogenotrophic microorganisms. Indeed, the constant electron supply on the surface of a conductive chimney allows a new energy source and long-range transfer between the electron donor (represented here by reduced molecules such as H_2S electrochemically oxidized on the inner surface of the chimney wall) and the electron acceptor (O_2, sulfur compounds, nitrate, metals) present all over the external surface of the chimney. This electrical current would thus allow primary colonizers to grow not just on all the surface but also in the chimney structure. These primary colonizers would release organic compounds used by the heterotrophic community for growth, as observed with the successive production and consumption of organic compounds in our experiments. Moreover, migrating out to larger potential growth surface would help to meet a wider range of physiological conditions through pH, temperature and oxidoreduction gradients. This allows a wider diversity of growth patterns than through chemolithoautotrophy, which is restricted to unstable and limited contact zones between reduced compounds (H_2, H_2S) in the hydrothermal fluid and electron acceptors around the hydrothermal chimneys, often precipitating together.

Conclusion

Taken together, the results found in this study converge into evidence of the ability of indigenous microorganisms from deep hydrothermal vents to grow using electric current and CO_2. This ability seems to be spread across diverse phylogenetic groups and to be coupled with diverse electron acceptors. Through their electro-litho-auto-trophic metabolism, *Archaeoglobaceae* strains produce and release organic compounds into their close environment, allowing the growth of

bioRxiv preprint doi: https://doi.org/10.1101/2020.11.11.377697; this version posted November 11, 2020. The copyright holder for this preprint (which was not certified by peer review) is the author/funder. All rights reserved. No reuse allowed without permission.

heterotrophic microorganisms, and ultimately enabling more and more diversity to develop over time. This metabolism could be one of the primary energies for the colonization of deep-sea hydrothermal chimneys and the development of a complex trophic network driving sustainable biodiversity. A similar mechanism could have occurred during the Hadean, allowing the emergence of life in hydrothermal environments by constant electron influx to the first proto-cells.

Experimental procedures

Sample collection and preparation

A hydrothermal chimney sample was collected on the acidic and iron-rich Capelinhos site on the Lucky Strike hydrothermal field (37°17.0'N, MAR) during the MoMARsat cruise in 2014 (http://dx.doi.org/10.17600/14000300) led by IFREMER (France) onboard R/V *Pourquoi Pas?* (Sarradin and Cannat, 2014). The sample (PL583-8) was collected by breaking off a piece of a high-temperature active black smoker using the submersible's robotic arm, and bringing it back to the surface in a decontaminated insulated box (http://video.ifremer.fr/video?id=9415). Onboard, chimney fragments were anaerobically crushed in an anaerobic chamber under H_2:N_2 (2.5:97.5) atmosphere (La Calhene, France), placed in flasks under anaerobic conditions (anoxic seawater at pH 7 with 0.5 mg L^{-1} of Na_2S and N_2:H_2:CO_2 (90:5:5) gas atmosphere), and stored at 4°C.

Prior to our experiments, pieces of the hydrothermal chimney were removed from the sulfidic seawater flask, crushed with a sterile mortar and pestle in an anaerobic chamber (Coy Laboratories, Grass Lake, MI), and distributed into anaerobic tubes for use in the various experiments.

Electrotrophic enrichment on nitrate, sulfate, and oxygen

MES were filled with 1.5 L of an amended sterile mineral medium as previously described (Pillot *et al.*, 2018) without yeast extract, and set at 80°C and pH 6.0 throughout on-platform monitoring. The electrode (cathode) composed of 20 cm^2 of carbon cloth was poised at the lowest potential

bioRxiv preprint doi: https://doi.org/10.1101/2020.11.11.377697; this version posted November 11, 2020. The copyright holder for this preprint (which was not certified by peer review) is the author/funder. All rights reserved. No reuse allowed without permission.

before initiation of abiotic current consumption (Supporting Information Fig S6) using SP-240 potentiostats and EC-Lab software (BioLogic, France). We thus used a potential of -590 mV *vs*(in the nitrate and sulfate experiments and -300 mV *vs* SHE in the oxygen experiment. A similar experiment at -300 mV vs SHE has been initiated in presence of sulfate (see SI Fig. S4) to confirm the growth of electrolithoautotroph microorganisms without any H_2 production possible. The electrode poised as cathode served as the sole electron donor for electrotroph growth. For the nitrate experiment, one system was supplemented with 4 mM of sodium nitrate. For the sulfate experiment, a second system was supplemented with 10 mM of sodium sulfate, and the cathodic chambers were sparged with N_2:CO_2 (90:10, 100 mL/min). For the oxygen experiment, a third system was sparged with N_2:CO_2:O_2 (80:10:10, 100 mL/min) with initially 10% oxygen as electron acceptor. All three systems were inoculated with 8 g of the crushed chimney (~0.5% (w/v)). Current consumption was monitored via the chronoamperometry method with current density and readings were taken every 10 s. An abiotic control without inoculation showed no current consumption during the same experiment period. CycloVoltammograms (scan rate: 20 mV/s) were analyzed using QSoas software (version 2.1). Coulombic efficiencies where calculates with the following equation:

$$CE\ (\%) = \frac{\mathrm{F} \cdot \mathrm{n_e} \cdot \Delta[\mathrm{P}] \cdot \mathrm{V_{catholyte}}}{\int_{t_0}^{t} \mathrm{I(t)} \cdot \mathrm{dt}} \cdot 100$$

I(t): current consumed between t_0 and t (A)

F: Faraday constant

n_e: number of moles of electrons presents per mole of product (mol)

Δ[P]: variation of the concentration of organic product between t_0 and t ($mol.L^{-1}$)

$V_{catholyte}$: volume of catholyte (L)

Identification and quantification of organic compound production

bioRxiv preprint doi: https://doi.org/10.1101/2020.11.11.377697; this version posted November 11, 2020. The copyright holder for this preprint (which was not certified by peer review) is the author/funder. All rights reserved. No reuse allowed without permission.

To identify and quantify the production of organic compounds from the biofilm, samples of liquid media were collected at the beginning and at the end of the experiment and analyzed by ^{1}H NMR spectroscopy. For this, 400 µL of each culture medium, were added to 200 µL of PBS solution prepared in D_2O (NaCl, 140 mM; KCl, 2.7 mM; KH_2PO_4, 1.5 mM; Na_2HPO_4, 8.1 mM, pH 7.4) supplemented with 0.5 mmol L^{-1} of trimethylsilylpropionic acid-*d*4 (TSP) as NMR reference. All the 1D ^{1}H NMR experiments were carried out at 300 K on a Bruker Avance spectrometer (Bruker, BioSpin Corporation, France) operating at 600 MHz for the ^{1}H frequency and equipped with a 5-mm BBFO probe.

Spectra were recorded using the 1D nuclear Overhauser effect spectroscopy pulse sequence (Trd-90°-T_1-90°-tm-90°-Taq) with a relaxation delay (Trd) of 12.5 s, a mixing time (tm) of 100 ms, and a T_1 of 4 µs. The sequence enables optimal suppression of the water signal that dominates the spectrum. We collected 128 free induction decays (FID) of 65,536 datapoints using a spectral width of 12 kHz and an acquisition time of 2.72 s. For all spectra, FIDs were multiplied by an exponential weighting function corresponding to a line broadening of 0.3 Hz and zero-filled before Fourier transformation. NMR spectra were manually phased using Topspin 3.5 software (Bruker Biospin Corporation, France) and automatically baseline-corrected and referenced to the TSP signal (δ = -0.015 ppm) using Chenomx NMR suite v7.5 software (Chenomx Inc., Canada). A 0.3 Hz line-broadening apodization was applied prior to spectral analysis, and ^{1}H-^{1}H TOCSY (Bax and Davis, 1985) and ^{1}H-^{13}C HSQC (Schleucher *et al.*, 1994) experiments were recorded on selected samples to identify the detected metabolites. Quantification of identified metabolites was done using Chenomx NMR suite v7.5 software (Chenomx Inc., Canada) using the TSP signal as the internal standard.

Biodiversity analysis

Taxonomic affiliation was carried out according to (Zhang *et al.*, 2016). DNA was extracted from 1 g of the crushed chimney and, at the end of each culture period, from scrapings of half of the WE

bioRxiv preprint doi: https://doi.org/10.1101/2020.11.11.377697; this version posted November 11, 2020. The copyright holder for this preprint (which was not certified by peer review) is the author/funder. All rights reserved. No reuse allowed without permission.

and from centrifuged pellets of 50 mL of spent media. The DNA extraction was carried out using the MoBio PowerSoil DNA isolation kit (Carlsbad, CA). The V4 region of the 16S rRNA gene was amplified using the universal primers 515F (5'-GTG CCA GCM GCC GCG GTA A-3') and 806R (5'-GGA CTA CNN GGG TAT CTA AT-3') (Bates *et al.*, 2011) with Taq&Load MasterMix (Promega). PCR reactions, qPCR, amplicon sequencing and taxonomic affiliation were carried as previously described (Pillot *et al.*, 2018). The qPCR results were expressed in copies number of 16s rRNA gene per gram of crushed chimney, per milliliter of liquid media or per cm^2 of surface of the electrode. To analyze alpha diversity, the OTU tables were rarefied to a sampling depth of 9410 sequences per library, and three metrics were calculated: the richness component, represented by number of OTUs observed, the Shannon index, representing total biodiversity, and the evenness index (Pielou's index), which measures distribution of individuals within species independently of species richness. Rarefaction curves (Supporting Information Fig. S7) for each enrichment approached an asymptote, suggesting that the sequencing depths were sufficient to capture overall microbial diversity in the studied samples. The phylogenetic tree was obtained with MEGA software v10.0.5 with the MUSCLE clustering algorithm and the Maximum Likelihood Tree Test with a Bootstrap method (2500 replications). The heatmap was obtained using RStudio software v3. The raw sequences for all samples can be found in the European Nucleotide Archive (accession number: PRJEB35427).

Acknowledgments

This work received financial support from the CNRS-sponsored national interdisciplinary research program (PEPS-ExoMod 2016). The authors thank Céline Rommevaux and Françoise Lesongeur for taking samples during the MOMARSAT 2014 cruise, the MIM platform (MIO, France) for providing access to their confocal microscopy facility, and the GeT-PlaGe platform (GenoToul, France) for help with DNA sequencing. The project leading to this publication received European FEDER funding under project "1166-39417. The authors declare no conflicts of interest.

bioRxiv preprint doi: https://doi.org/10.1101/2020.11.11.377697; this version posted November 11, 2020. The copyright holder for this preprint (which was not certified by peer review) is the author/funder. All rights reserved. No reuse allowed without permission.

495

bioRxiv preprint doi: https://doi.org/10.1101/2020.11.11.377697; this version posted November 11, 2020. The copyright holder for this preprint (which was not certified by peer review) is the author/funder. All rights reserved. No reuse allowed without permission.

References

Alain, K., Zbinden, M., Bris, N.L., Lesongeur, F., Quérellou, J., Gaill, F., and Cambon-Bonavita, M.-A. (2004) Early steps in microbial colonization processes at deep-sea hydrothermal vents. *Environ Microbiol* **6**: 227–241.

Albuquerque, L. and Costa, M.S. da (2014) The Family *Thermaceae*. In *The Prokaryotes*. Springer, Berlin, Heidelberg, pp. 955–987.

Bates, S.T., Berg-Lyons, D., Caporaso, J.G., Walters, W.A., Knight, R., and Fierer, N. (2011) Examining the global distribution of dominant archaeal populations in soil. *ISME J* **5**: 908–917.

Bax, A. and Davis, D.G. (1985) MLEV-17-based two-dimensional homonuclear magnetization transfer spectroscopy. *J Magn Reson 1969* **65**: 355–360.

Berg, I.A., Kockelkorn, D., Ramos-Vera, W.H., Say, R.F., Zarzycki, J., Hügler, M., et al. (2010) Autotrophic carbon fixation in archaea. *Nat Rev Microbiol* **8**: 447–460.

Björkqvist, S., Ansell, R., Adler, L., and Lidén, G. (1997) Physiological response to anaerobicity of glycerol-3-phosphate dehydrogenase mutants of Saccharomyces cerevisiae. *Appl Env Microbiol* **63**: 128–132.

Brileya, K. and Reysenbach, A.-L. (2014) The Class *Archaeoglobi*. In *The Prokaryotes*. Springer, Berlin, Heidelberg, pp. 15–23.

Corliss, J.B. and Ballard, R.D. (1977) Oasis of life in the cold abyss. *Nat Geogr Mag* **152**: 440–453.

Corre, E., Reysenbach, A.-L., and Prieur, D. (2001) ε-Proteobacterial diversity from a deep-sea hydrothermal vent on the Mid-Atlantic Ridge. *FEMS Microbiol Lett* **205**: 329–335.

Dahle, H., Le Moine Bauer, S., Baumberger, T., Stokke, R., Pedersen, R.B., Thorseth, I.H., and Steen, I.H. (2018) Energy landscapes in hydrothermal chimneys shape distributions of primary producers. *Front Microbiol* **9**:.

Desai, J.V., Bruno, V.M., Ganguly, S., Stamper, R.J., Mitchell, K.F., Solis, N., et al. (2013) Regulatory Role of Glycerol in Candida albicans Biofilm Formation. *mBio* **4**:.

Droffner, M.L., Brinton, W.F., and Evans, E. (1995) Evidence for the prominence of well characterized mesophilic bacteria in thermophilic (50–70°C) composting environments. *Biomass Bioenergy* **8**: 191–195.

Fast, A.G. and Papoutsakis, E.T. (2012) Stoichiometric and energetic analyses of non-photosynthetic CO2-fixation pathways to support synthetic biology strategies for production of fuels and chemicals. *Curr Opin Chem Eng* **1**: 380–395.

Fuchs, G. (2011) Alternative Pathways of Carbon Dioxide Fixation: Insights into the Early Evolution of Life? *Annu Rev Microbiol* **65**: 631–658.

Furdui, C. and Ragsdale, S.W. (2000) The role of pyruvate ferredoxin oxidoreductase in pyruvate synthesis during autotrophic growth by the Wood-Ljungdahl pathway. *J Biol Chem* **275**: 28494–28499.

Hamilton, W.A. (1987) Biofilms : Microbial interactions and metabolic activities. *Ecol Microb Communities* 361–385.

Henstra, A.M., Dijkema, C., and Stams, A.J.M. (2007) *Archaeoglobus fulgidus* couples CO oxidation to sulfate reduction and acetogenesis with transient formate accumulation: The CO metabolism of *A. fulgidus*. *Environ Microbiol* **9**: 1836–1841.

Hocking, W.P., Roalkvam, I., Magnussen, C., Stokke, R., and Steen, I.H. (2015) Assessment of the Carbon Monoxide Metabolism of the Hyperthermophilic Sulfate-Reducing Archaeon *Archaeoglobus fulgidus* VC-16 by Comparative Transcriptome Analyses. *Archaea* **2015**: 1–12.

Huber, H. and Stetter, K.O. (2015) Desulfurococcales ord. nov. In *Bergey's Manual of Systematics of Archaea and Bacteria*. American Cancer Society, pp. 1–2.

Huber, J.A., Butterfield, D.A., and Baross, J.A. (2003) Bacterial diversity in a subseafloor habitat following a deep-sea volcanic eruption. *FEMS Microbiol Ecol* **43**: 393–409.

Huber, J.A., Butterfield, D.A., and Baross, J.A. (2002) Temporal changes in archaeal diversity and chemistry in a mid-ocean ridge subseafloor habitat. *Appl Environ Microbiol* **68**: 1585–1594.

bioRxiv preprint doi: https://doi.org/10.1101/2020.11.11.377697; this version posted November 11, 2020. The copyright holder for this preprint (which was not certified by peer review) is the author/funder. All rights reserved. No reuse allowed without permission.

548 Ishii, T., Kawaichi, S., Nakagawa, H., Hashimoto, K., and Nakamura, R. (2015) From
549 chemolithoautotrophs to electrolithoautotrophs: CO2 fixation by Fe(II)-oxidizing bacteria
550 coupled with direct uptake of electrons from solid electron sources. *Front Microbiol* **6**:.
551 Jaeschke, A., Jørgensen, S.L., Bernasconi, S.M., Pedersen, R.B., Thorseth, I.H., and Früh-Green,
552 G.L. (2012) Microbial diversity of Loki's Castle black smokers at the Arctic Mid-Ocean
553 Ridge. *Geobiology* **10**: 548–561.
554 Jia, R., Yang, D., Xu, D., and Gu, T. (2018) Carbon steel biocorrosion at 80 °C by a thermophilic
555 sulfate reducing archaeon biofilm provides evidence for its utilization of elemental iron as
556 electron donor through extracellular electron transfer. *Corros Sci* **145**: 47–54.
557 Kato, S., Hashimoto, K., and Watanabe, K. (2012) Microbial interspecies electron transfer via
558 electric currents through conductive minerals. *Proc Natl Acad Sci* **109**: 10042–10046.
559 Lai, B., Yu, S., Bernhardt, P.V., Rabaey, K., Virdis, B., and Krömer, J.O. (2016) Anoxic metabolism
560 and biochemical production in Pseudomonas putida F1 driven by a bioelectrochemical
561 system. *Biotechnol Biofuels* **9**: 39.
562 Lim, S.S., Yu, E.H., Daud, W.R.W., Kim, B.H., and Scott, K. (2017) Bioanode as a limiting factor
563 to biocathode performance in microbial electrolysis cells. *Bioresour Technol* **238**: 313–324.
564 Lin, T.J., Ver Eecke, H.C., Breves, E.A., Dyar, M.D., Jamieson, J.W., Hannington, M.D., et al.
565 (2016) Linkages between mineralogy, fluid chemistry, and microbial communities within
566 hydrothermal chimneys from the Endeavour Segment, Juan de Fuca Ridge:
567 GEOMICROBIOLOGY OF HYDROTHERMAL CHIMNEYS. *Geochem Geophys*
568 *Geosystems* **17**: 300–323.
569 Lovley, D.R. (2017) Syntrophy goes electric: Direct interspecies electron transfer. *Annu Rev*
570 *Microbiol* **71**: 643–664.
571 Lyons, C.M., Justin, P., Colby, J., and Williams, E. (1984) Isolation, characterization and autotrophic
572 metabolism of a moderately thermophilic carboxydobacterium, *Pseudomonas*
573 *thermocarboxydovorans* sp. nov. *Microbiology* **130**: 1097–1105.
574 Manzella, M.P., Holmes, D.E., Rocheleau, J.M., Chung, A., Reguera, G., and Kashefi, K. (2015) The
575 complete genome sequence and emendation of the hyperthermophilic, obligate iron-reducing
576 archaeon "Geoglobus ahangari" strain 234T. *Stand Genomic Sci* **10**: 77.
577 Marshall, C.W., Ross, D.E., Fichot, E.B., Norman, R.S., and May, H.D. (2013) Long-term Operation
578 of Microbial Electrosynthesis Systems Improves Acetate Production by Autotrophic
579 Microbiomes. *Environ Sci Technol* **47**: 6023–6029.
580 Maruthupandy, M., Anand, M., Maduraiveeran, G., Beevi, A.S.H., and Priya, R.J. (2015) Electrical
581 conductivity measurements of bacterial nanowires from Pseudomonas aeruginosa. *Adv Nat*
582 *Sci Nanosci Nanotechnol* **6**: 045007.
583 Nercessian, O., Reysenbach, A.-L., Prieur, D., and Jeanthon, C. (2003) Archaeal diversity associated
584 with in situ samplers deployed on hydrothermal vents on the East Pacific Rise (13°N).
585 *Environ Microbiol* **5**: 492–502.
586 Palleroni, N.J. (2015) Pseudomonas. In *Bergey's Manual of Systematics of Archaea and Bacteria*.
587 American Cancer Society, pp. 1–1.
588 Pillot, G., Davidson, S., Auria, R., Combet-Blanc, Y., Godfroy, A., and Liebgott, P.-P. (2019)
589 Production of Current by Syntrophy Between Exoelectrogenic and Fermentative
590 Hyperthermophilic Microorganisms in Heterotrophic Biofilm from a Deep-Sea
591 Hydrothermal Chimney. *Microb Ecol*.
592 Pillot, G., Frouin, E., Pasero, E., Godfroy, A., Combet-Blanc, Y., Davidson, S., and Liebgott, P.-P.
593 (2018) Specific enrichment of hyperthermophilic electroactive *Archaea* from deep-sea
594 hydrothermal vent on electrically conductive support. *Bioresour Technol* **259**: 304–311.
595 Pous, N., Carmona-Martínez, A.A., Vilajeliu-Pons, A., Fiset, E., Bañeras, L., Trably, E., et al. (2016)
596 Bidirectional microbial electron transfer: Switching an acetate oxidizing biofilm to nitrate
597 reducing conditions. *Biosens Bioelectron* **75**: 352–358.
598 Reimers, C.E., Girguis, P., Stecher, H.A., Tender, L.M., Ryckelynck, N., and Whaling, P. (2006)
599 Microbial fuel cell energy from an ocean cold seep. *Geobiology* **4**: 123–136.

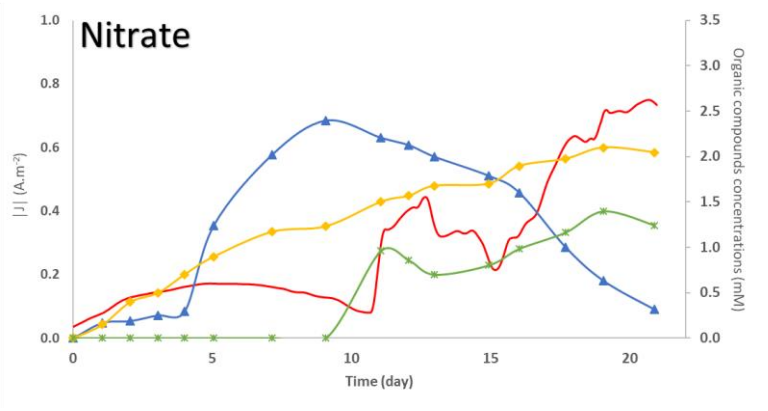
bioRxiv preprint doi: https://doi.org/10.1101/2020.11.11.377697; this version posted November 11, 2020. The copyright holder for this preprint (which was not certified by peer review) is the author/funder. All rights reserved. No reuse allowed without permission.

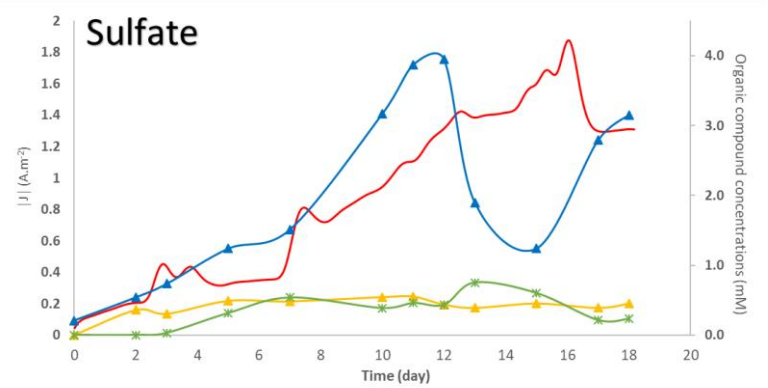
600 Reysenbach, A.-L., Longnecker, K., and Kirshtein, J. (2000) Novel bacterial and archaeal lineages
601 from an in situ growth chamber deployed at a Mid-Atlantic Ridge hydrothermal vent. *Appl*
602 *Environ Microbiol* **66**: 3798–3806.
603 Salter, S.J., Cox, M.J., Turek, E.M., Calus, S.T., Cookson, W.O., Moffatt, M.F., et al. (2014) Reagent
604 and laboratory contamination can critically impact sequence-based microbiome analyses.
605 *BMC Biol* **12**: 87.
606 Sarradin, P.-M. and Cannat, M. (2014) MOMARSAT2014 cruise,Pourquoi pas ? R/V.
607 Schleucher, J., Schwendinger, M., Sattler, M., Schmidt, P., Schedletzky, O., Glaser, S.J., et al. (1994)
608 A general enhancement scheme in heteronuclear multidimensional NMR employing pulsed
609 field gradients. *J Biomol NMR* **4**: 301–306.
610 Schrenk, M.O., Kelley, D.S., Delaney, J.R., and Baross, J.A. (2003) Incidence and diversity of
611 microorganisms within the walls of an active deep-sea sulfide chimney. *Appl Environ*
612 *Microbiol* **69**: 3580–3592.
613 Shemesh, M. and Chai, Y. (2013) A Combination of Glycerol and Manganese Promotes Biofilm
614 Formation in Bacillus subtilis via Histidine Kinase KinD Signaling. *J Bacteriol* **195**: 2747–
615 2754.
616 Shen, H.-B., Yong, X.-Y., Chen, Y.-L., Liao, Z.-H., Si, R.-W., Zhou, J., et al. (2014) Enhanced
617 bioelectricity generation by improving pyocyanin production and membrane permeability
618 through sophorolipid addition in Pseudomonas aeruginosa-inoculated microbial fuel cells.
619 *Bioresour Technol* **167**: 490–494.
620 Sokolova, T. and Lebedinsky, A. (2013) CO-Oxidizing Anaerobic Thermophilic Prokaryotes. In
621 *Thermophilic Microbes in Environmental and Industrial Biotechnology: Biotechnology of*
622 *Thermophiles*. Satyanarayana, T., Littlechild, J., and Kawarabayasi, Y. (eds). Dordrecht:
623 Springer Netherlands, pp. 203–231.
624 Takai, K., Gamo, T., Tsunogai, U., Nakayama, N., Hirayama, H., Nealson, K.H., and Horikoshi, K.
625 (2004) Geochemical and microbiological evidence for a hydrogen-based, hyperthermophilic
626 subsurface lithoautotrophic microbial ecosystem (HyperSLiME) beneath an active deep-sea
627 hydrothermal field. *Extremophiles* **8**: 269–282.
628 Vorholt, J.A., Hafenbradl, D., Stetter, K.O., and Thauer, R.K. (1997) Pathways of autotrophic CO 2
629 fixation and of dissimilatory nitrate reduction to N 2 O in Ferroglobus placidus. *Arch*
630 *Microbiol* **167**: 19–23.
631 Vos, P.D. (2015) Bacillales. In *Bergey's Manual of Systematics of Archaea and Bacteria*. American
632 Cancer Society, pp. 1–1.
633 Wirth, R. (2017) Colonization of black smokers by hyperthermophilic microorganisms. *Trends*
634 *Microbiol* **25**: 92–99.
635 Wirth, R., Luckner, M., and Wanner, G. (2018) Validation of a hypothesis: Colonization of black
636 smokers by hyperthermophilic microorganisms. *Front Microbiol* **9**: 524.
637 Yamamoto, M., Nakamura, R., Kasaya, T., Kumagai, H., Suzuki, K., and Takai, K. (2017)
638 Spontaneous and Widespread Electricity Generation in Natural Deep-Sea Hydrothermal
639 Fields. *Angew Chem Int Ed* **56**: 5725–5728.
640 Yilmazel, Y.D., Zhu, X., Kim, K.-Y., Holmes, D.E., and Logan, B.E. (2018) Electrical current
641 generation in microbial electrolysis cells by hyperthermophilic archaea *Ferroglobus*
642 *placidus* and *Geoglobus ahangari*. *Bioelectrochemistry* **119**: 142–149.
643 Zhang, L., Kang, M., Xu, Jiajun, Xu, Jian, Shuai, Y., Zhou, X., et al. (2016) Bacterial and archaeal
644 communities in the deep-sea sediments of inactive hydrothermal vents in the Southwest India
645 Ridge. *Sci Rep* **6**:.
646

647

bioRxiv preprint doi: https://doi.org/10.1101/2020.11.11.377697; this version posted November 11, 2020. The copyright holder for this preprint (which was not certified by peer review) is the author/funder. All rights reserved. No reuse allowed without permission.

Figures





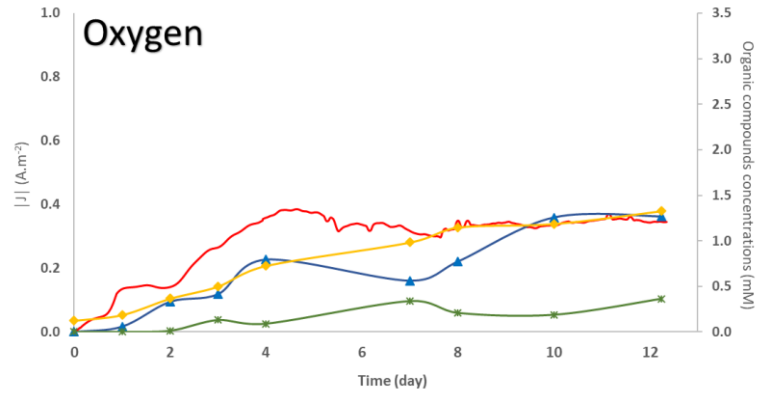
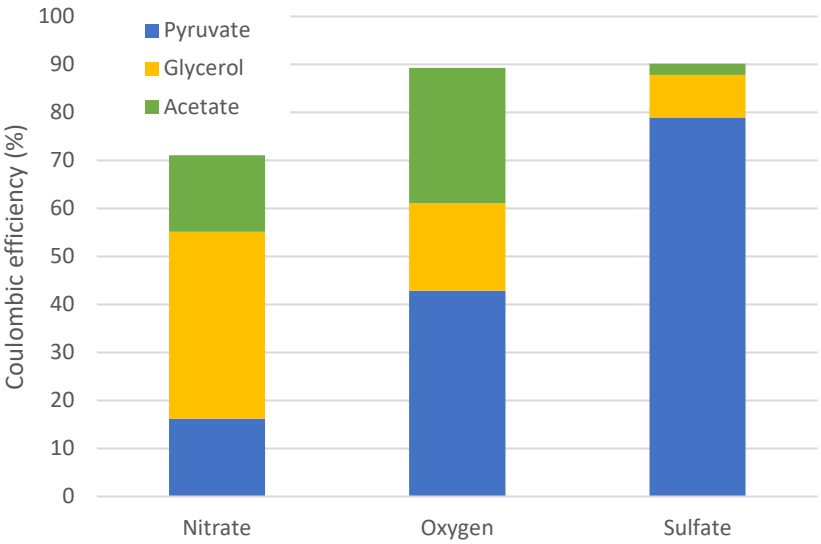


Figure 1. Current consumption (red continuous line); pyruvate (blue triangle), glycerol (yellow square) and acetate (green cross) productions over time of culture for each electron-acceptor experiment. The current was obtained from a poised electrode at -590 mV vs SHE for nitrate and sulfate experiments and -300 mV vs SHE for oxygen.

bioRxiv preprint doi: https://doi.org/10.1101/2020.11.11.377697; this version posted November 11, 2020. The copyright holder for this preprint (which was not certified by peer review) is the author/funder. All rights reserved. No reuse allowed without permission.



657

658 **Figure 2.** Coulombic efficiency for organic products in presence of the different electron

659 acceptors.

660

bioRxiv preprint doi: https://doi.org/10.1101/2020.11.11.377697; this version posted November 11, 2020. The copyright holder for this preprint (which was not certified by peer review) is the author/funder. All rights reserved. No reuse allowed without permission.

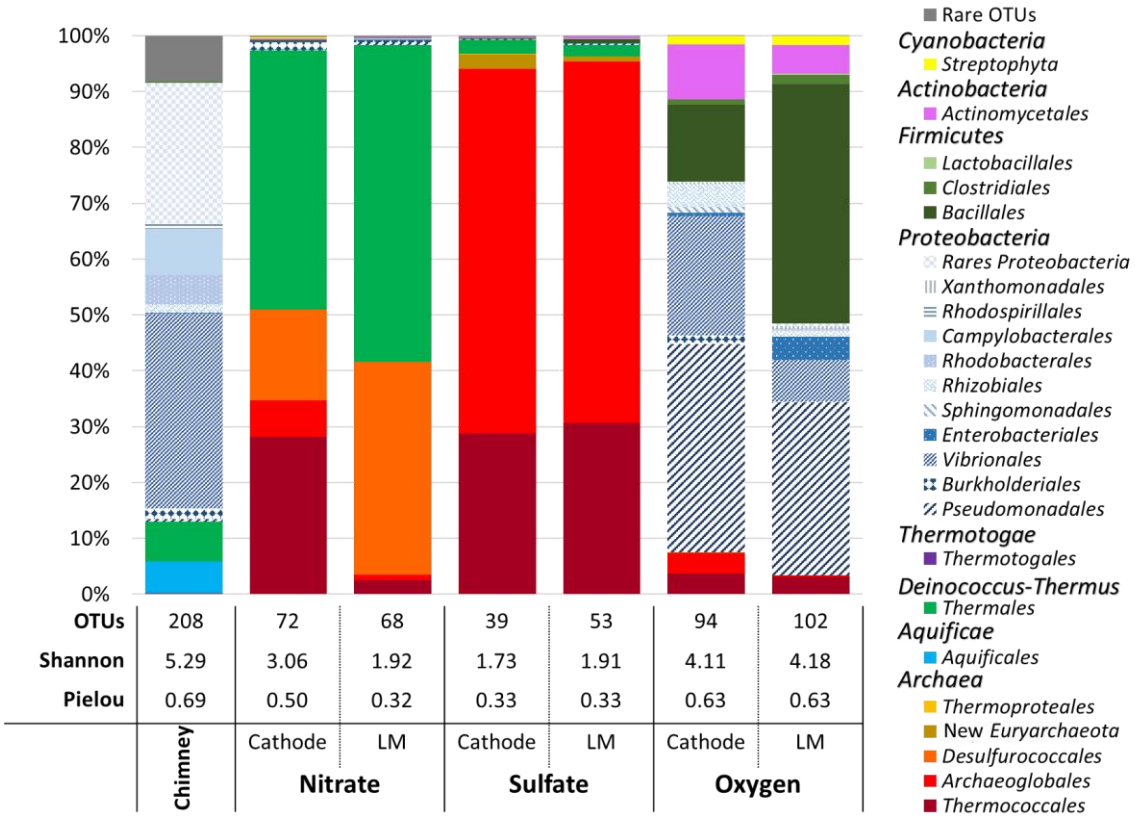
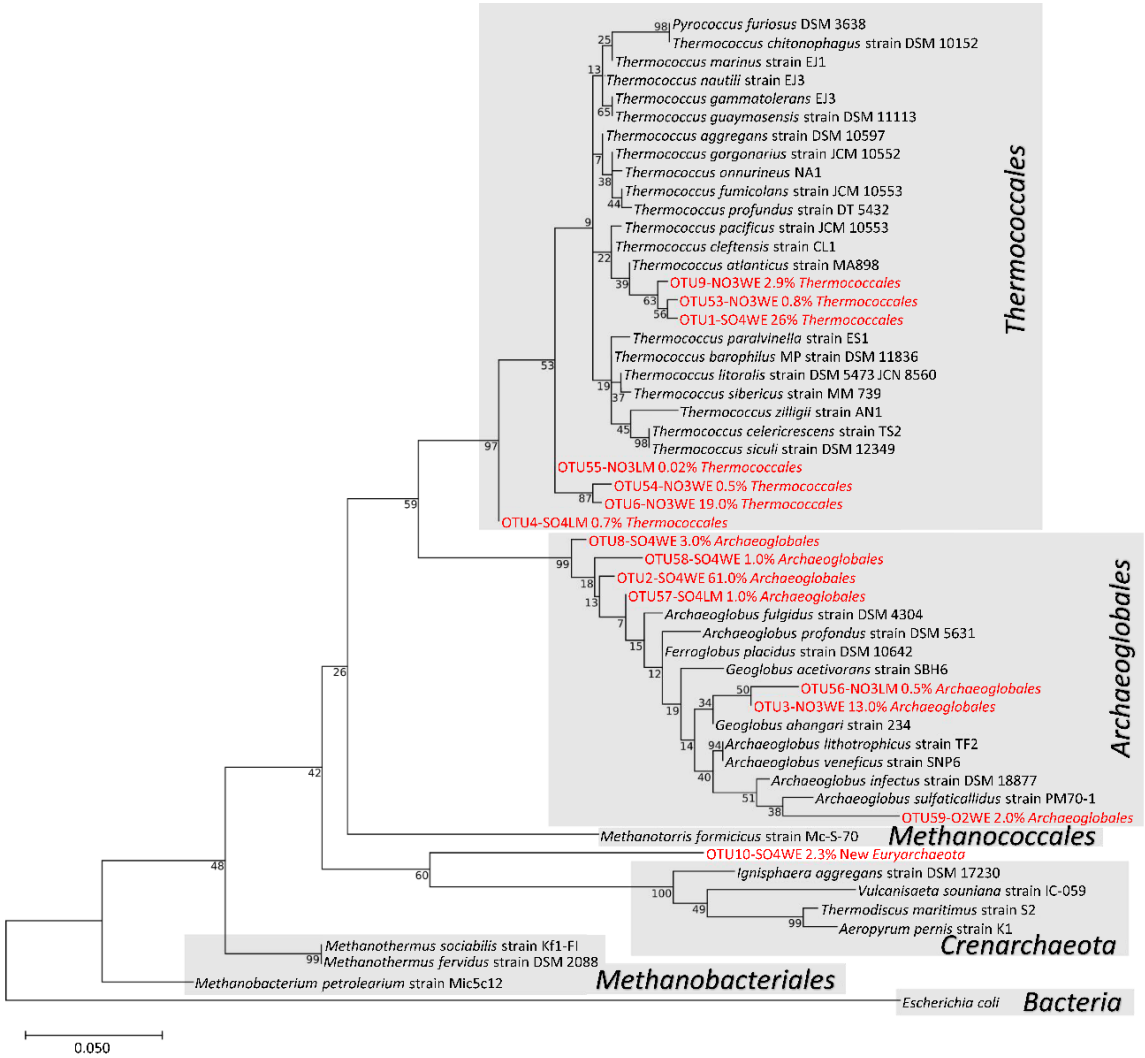


Figure 3. Dominant taxonomic affiliation at order level and biodiversity indices of microbial communities from a crushed chimney sample from Capelinhos vent site (Lucky Strike hydrothermal vent field), as plotted on the cathode and liquid media (LM) after the weeks of culture. OTUs representing less than 1% of total sequences of the samples are pooled as 'Rare OTUs'.

bioRxiv preprint doi: https://doi.org/10.1101/2020.11.11.377697; this version posted November 11, 2020. The copyright holder for this preprint (which was not certified by peer review) is the author/funder. All rights reserved. No reuse allowed without permission.



669 **Figure 4.** Maximum Likelihood phylogenetic tree of archaeal OTUs retrieved on various

670 enrichments on the 293pb 16S fragment obtained in the barcoding 16S method (LM: Liquid

671 Media; WE: Working Electrode, cathode). Numbers at nodes represent bootstrap values inferred

672 by MEGAX. Scale bars represent the average number of substitutions per site.

673

674

675

bioRxiv preprint doi: https://doi.org/10.1101/2020.11.11.377697; this version posted November 11, 2020. The copyright holder for this preprint (which was not certified by peer review) is the author/funder. All rights reserved. No reuse allowed without permission.

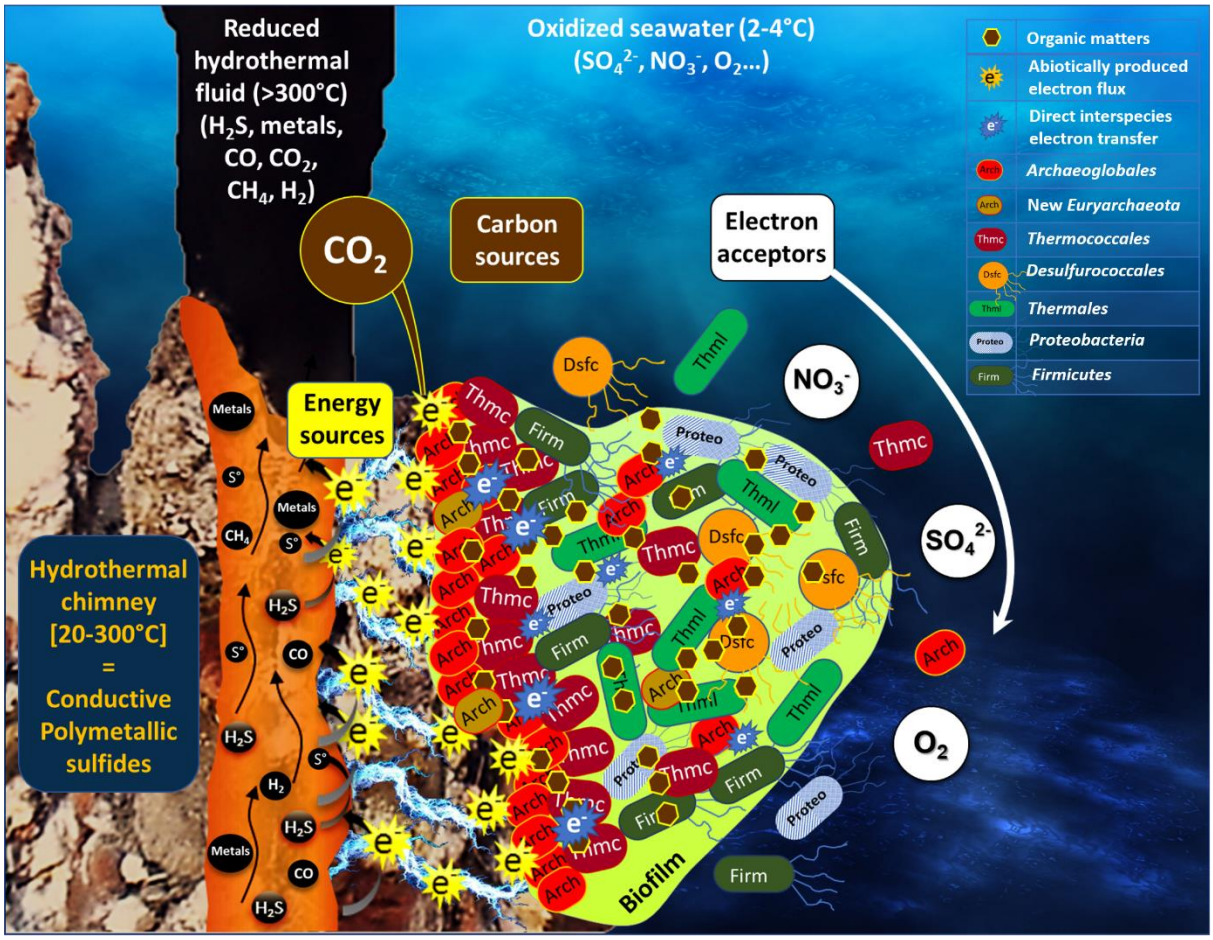
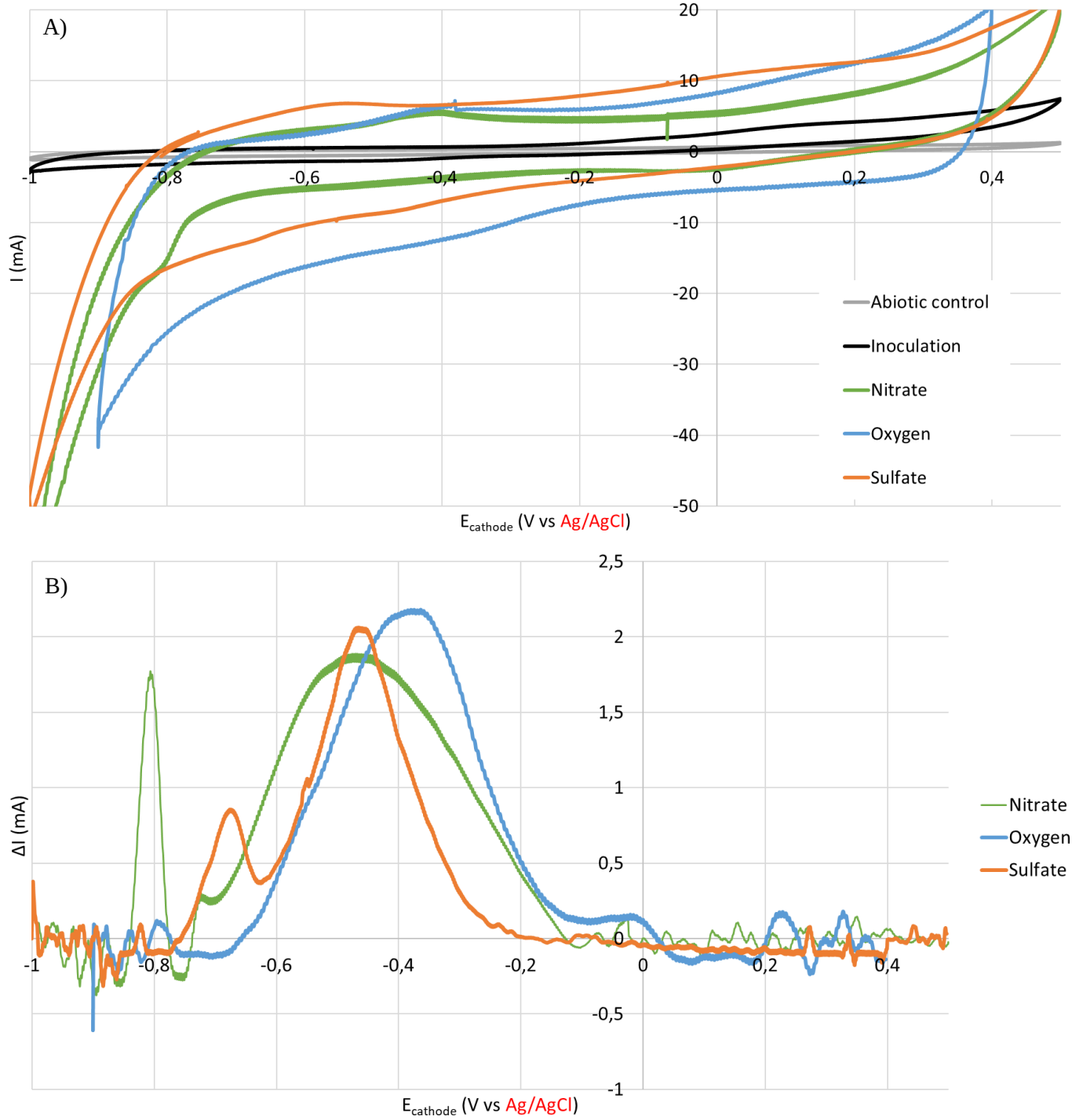


Figure 5: Schematic representation of microbial colonization of iron-rich hydrothermal chimney (Capelinhos site on the Lucky Strike hydrothermal field) by electrolithoautotrophic microorganisms. The production of an abiotic electrical current by potential differences between the reduced hydrothermal fluid (H_2S, metals, CO, CH_4, H_2…) and oxidized seawater (O_2, SO_4^{2-}, NO_3^{2-}) (Yamamoto et al. 2017) leads to the formation of electron flux moving towards the chimney surface. This electrons flux can serve directly as an energy source to enable the growth of electrolithoautotrophic and hyperthermophilic *Archaeolgobales* using the CO_2 as carbon source and nitrate and/or sulfate as electron acceptors. In the absence of a usable electron acceptor, *Archaeoglobales* would be likely to perform direct interspecies electron transfer to ensure their growth. The electron acceptor fluctuations, correlated to the continual influx of electric current would favor the production of organic matters (amino acid, formate, pyruvate, glycerol...) by the *Archaeoglobales*. This organic matter is then used by heterotrophic microorganisms by fermentation or respiration (anaerobic or aerobic) thus providing the primal food web initially present into the hydrothermal ecosystems. *The electrical current also could favor the electrolysis water leading to the abiotic H_2 production (not measurable in our abiotic conditions), which would serve as chemical energy source*. Arch: *Achaeoglobales*; Thmc: *Thermococcales*; Dsfc: *Desulfurococcales*; Thml: *Thermales*; Prot: *Proteobacteria*; Firm: *Firmicute*; NO_3^-: nitrate; SO_4^{2-}: sulfate; O_2: dioxygen; CH_4: Methane; CO_2: Carbon Dioxide; CO: Carbon monoxide; H_2S : Hydrogen sulfide ; S°: sulfur; Metals: Fe, Mn, Cu, Zn…

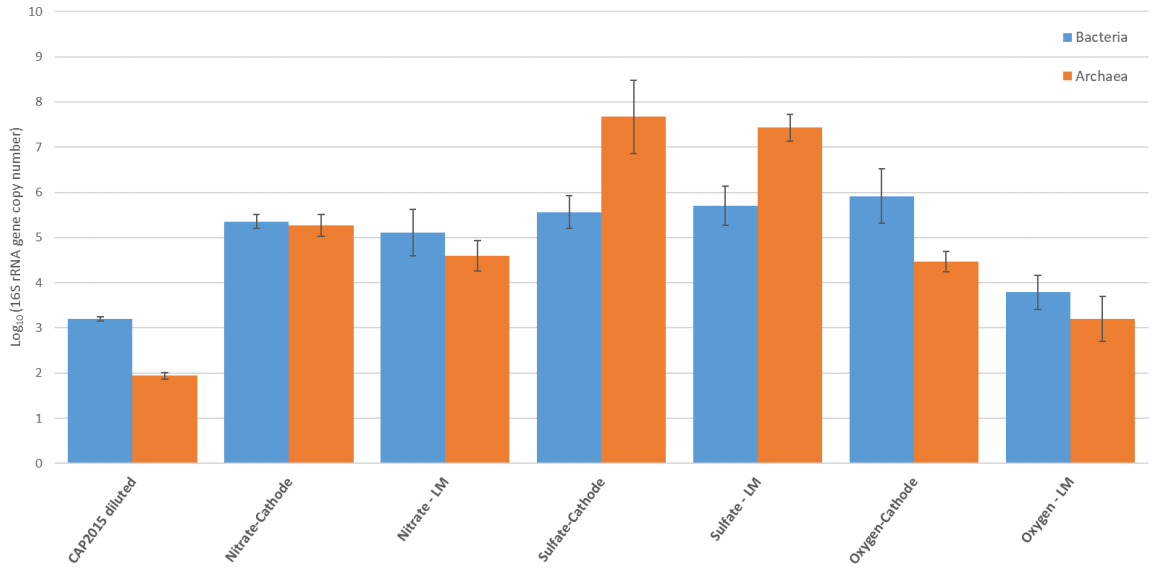
bioRxiv preprint doi: https://doi.org/10.1101/2020.11.11.377697; this version posted November 11, 2020. The copyright holder for this preprint (which was not certified by peer review) is the author/funder. All rights reserved. No reuse allowed without permission.

SUPPLEMENTARY INFORMATION



Supplementary Information Figure S1: A) CyclicVoltammograms (scan rate = 20 mV/s) of the abiotic control, and of the experiments at inoculation time and after 30 days for each condition (Nitrate, Oxygen and Sulfate). B) Reduction peaks extracted from CyclicVoltammograms (scan rate = 20 mV/s) where the baseline have been substracted with the sofware QSoas. The ΔI of reduction peaks are expressed in inversed values. Cyclovoltammograms carried out with a 3 M Ag/AgCl reference electrode (E= +0.165 V vs SHE at 80°C).

bioRxiv preprint doi: https://doi.org/10.1101/2020.11.11.377697; this version posted November 11, 2020. The copyright holder for this preprint (which was not certified by peer review) is the author/funder. All rights reserved. No reuse allowed without permission.



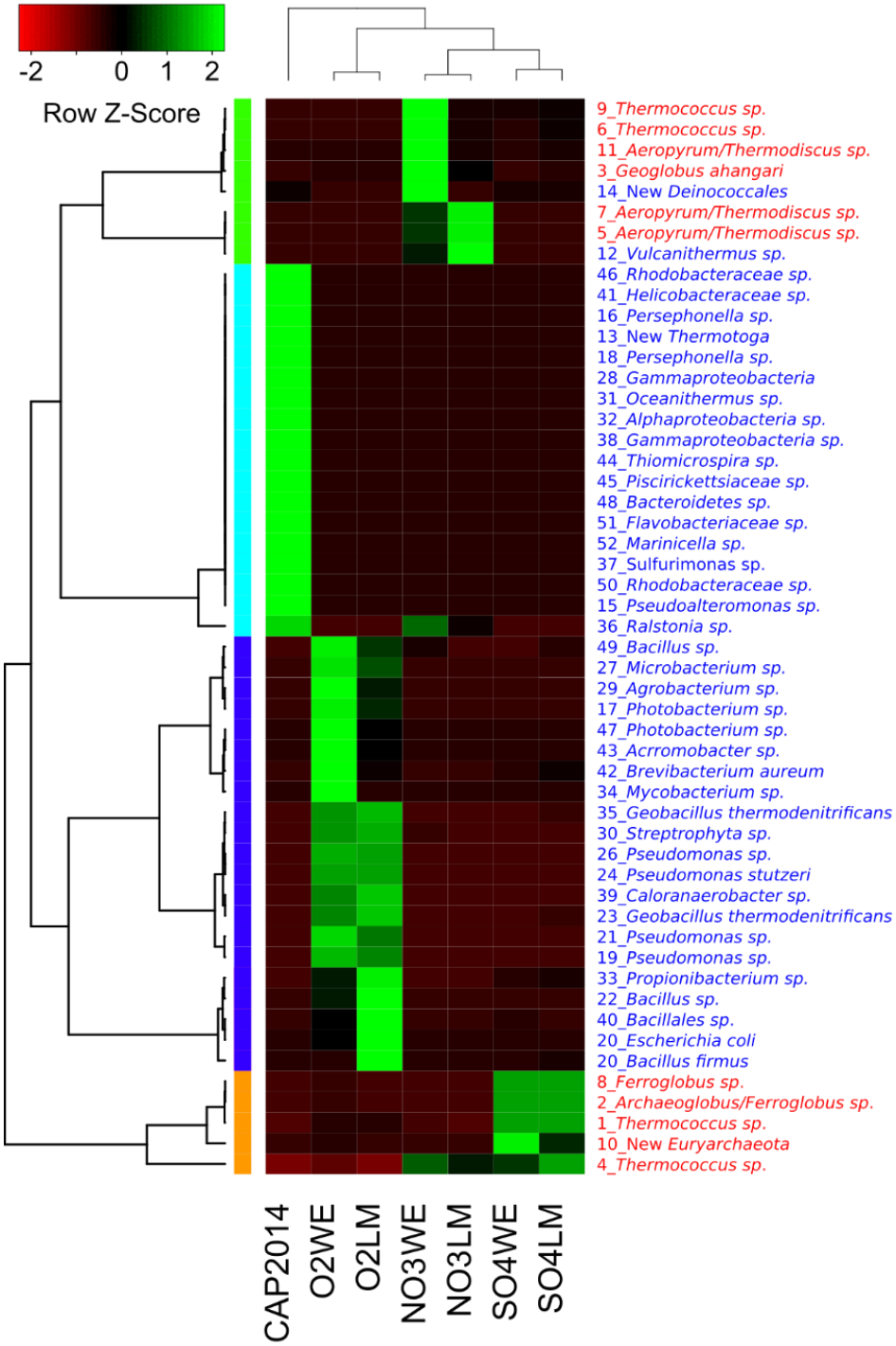
718

719 **Supplementary Information Figure S2.** Quantification of 16S rRNA gene copies from Bacteria

720 (blue) or Archaea (orange) per gram of crushed chimney, per milliliter of liquid or per cm^2 of

721 working electrode. Error bar represent the standard deviation obtained on triplicates.

bioRxiv preprint doi: https://doi.org/10.1101/2020.11.11.377697; this version posted November 11, 2020. The copyright holder for this preprint (which was not certified by peer review) is the author/funder. All rights reserved. No reuse allowed without permission.



Supplementary Information Figure S3. Heatmap representation of the distribution of dominant OTUs (>0.05%) over the different electron acceptors (LM: Liquid Media; WE: Working Electrode, cathode). OTUs and samples clustering were performed with centroid average method and with Pearson distance measurement method. The red taxa represent the Archaea members and blue taxa, the Bacteria.

bioRxiv preprint doi: https://doi.org/10.1101/2020.11.11.377697; this version posted November 11, 2020. The copyright holder for this preprint (which was not certified by peer review) is the author/funder. All rights reserved. No reuse allowed without permission.

728

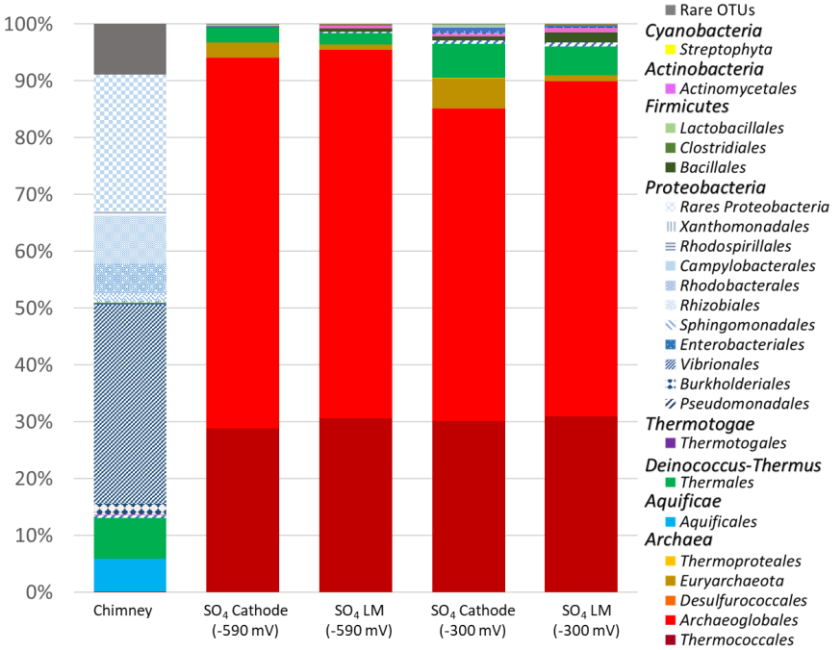
729

730

731

bioRxiv preprint doi: https://doi.org/10.1101/2020.11.11.377697; this version posted November 11, 2020. The copyright holder for this preprint (which was not certified by peer review) is the author/funder. All rights reserved. No reuse allowed without permission.

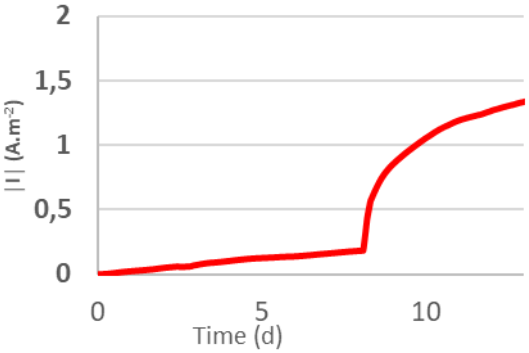
A)



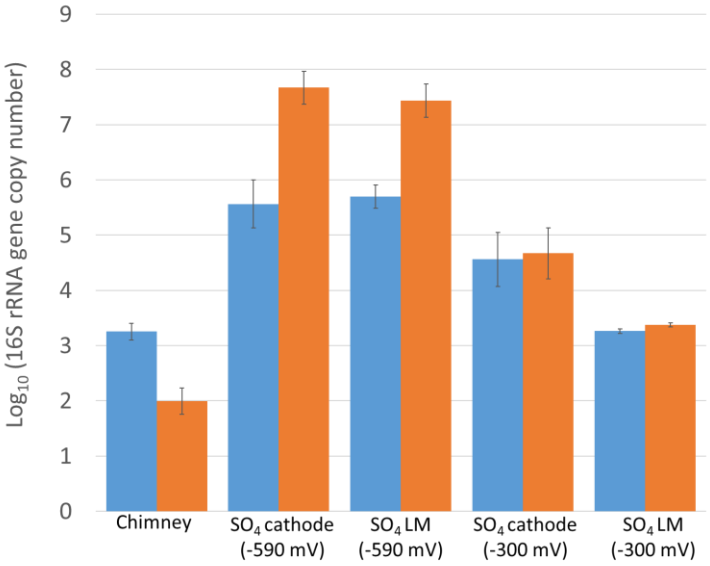
B)

Potential (ESH)	-300 mV
Growth time	24 days
T°C	80
|i| (A/m²)max	1.38
Electron acceptor	Sulfate (10 mM)
culture medium	sea water
inoculum CAP2014	Part of chimney (1% w/v)

C)

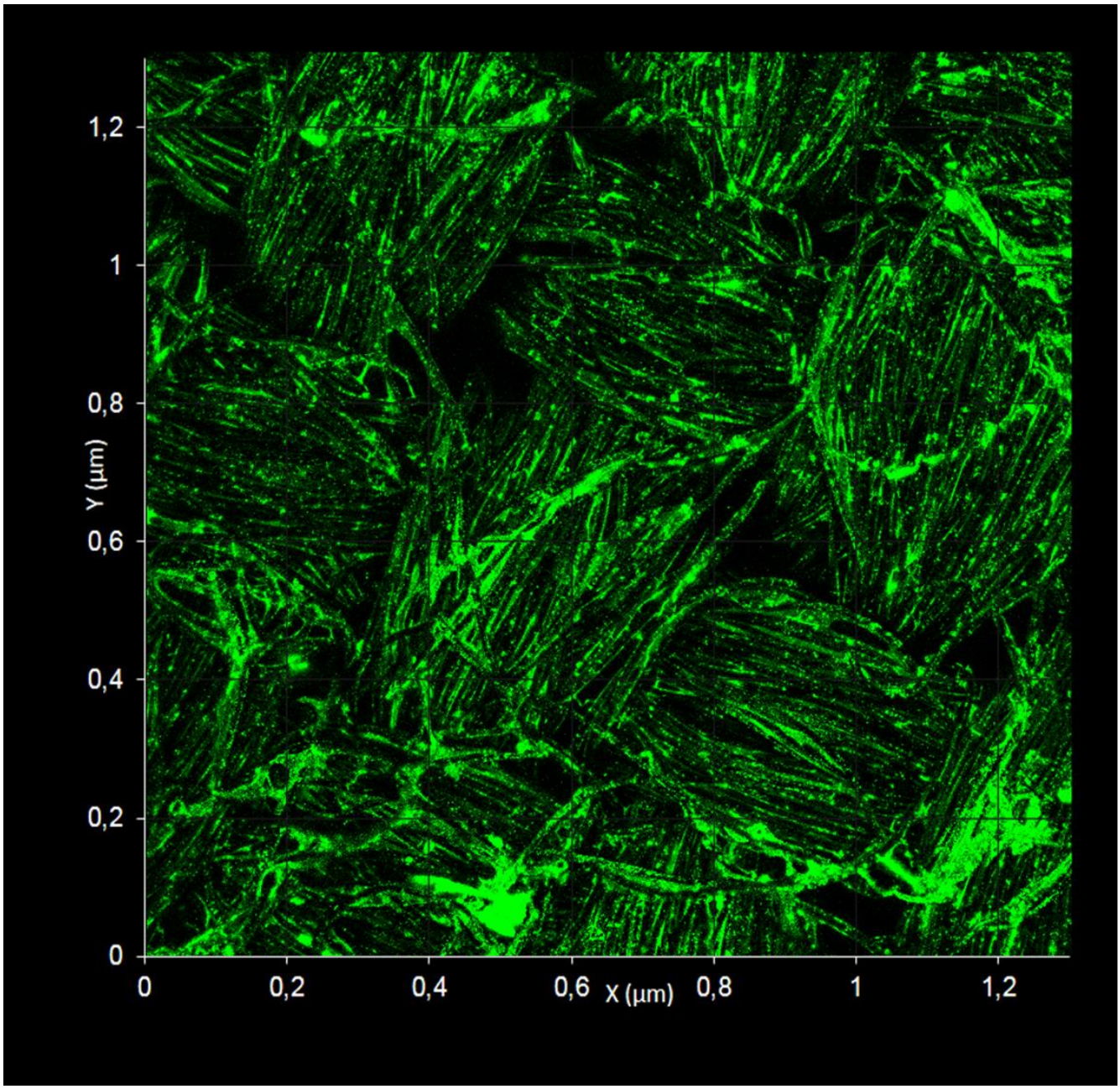


D)



Supplementary Information Figure S4: A) Biodiversity comparisons developing it on poised cathode at -590 mV and -300 mV vs SHE in presence of sulfate. B) Parameters of growth with the cathode poised at -300 mV vs SHE. C) current consumption correlated to the growth of biofilm. D) Quantification of 16S rRNA gene copies from Bacteria (blue) or Archaea (orange) per gram of crushed chimney, per milliliter of liquid or per cm² of cathode.

bioRxiv preprint doi: https://doi.org/10.1101/2020.11.11.377697; this version posted November 11, 2020. The copyright holder for this preprint (which was not certified by peer review) is the author/funder. All rights reserved. No reuse allowed without permission.

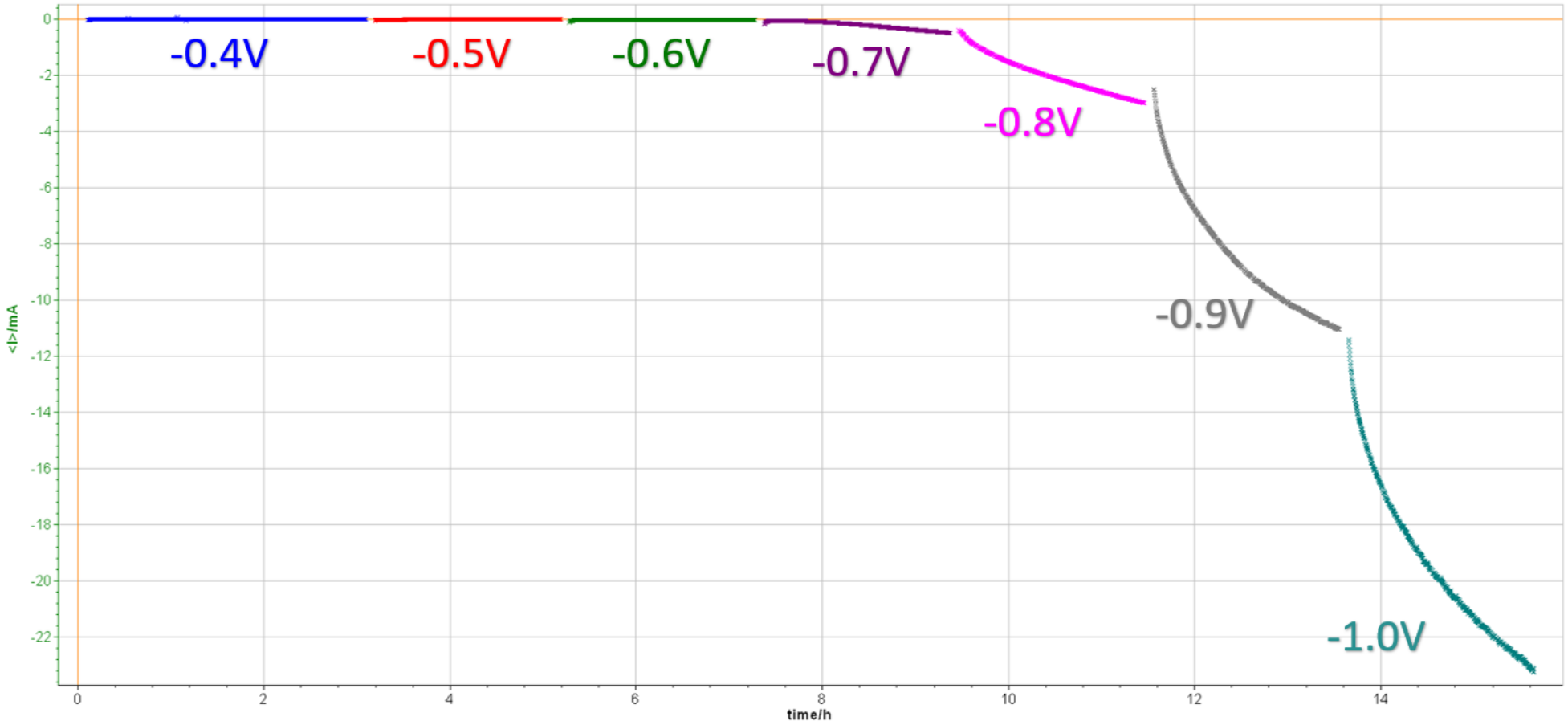


Supplementary information Figure S5: Representative confocal microscopy of the biofilm after 30 days of experiment on nitrate as electron acceptor. The green signal, corresponding to cells stained with Syto9 dye, allow to show the biofilm covering the interwoven carbon fibers.

Time (days)	Benzoate like	Methanol	Formate	Cystine	Acetoacetate	Lactate	Threonine	Succinate	Ethanol	Alanine	Acetamide	2-Aminoisobutyric acid	3-hydroxyisovalerate
0	0,0056	0,0032	0,0085	0,0123	0,024	0,0066	0,0019	0,0013	0,0022	0	0	0,0048	0,0046
1	0	0	0,0615	0,0355	0	0,03	0,0115	0	0,177	0	0	0,067	0,0375
2	0,0294	0	0,0084	0,0302	0	0,024	0,0026	0,0022	0,0406	0	0	0	0,0076
3	0,0198	0,0108	0,0549	0,0237	0	0,015	0,0036	0	0,0375	0,0108	0	0,0051	0,0282
4	0,0242	0,1606	0,0218	0,0306	0	0,0106	0,004	0	0.0425	0,012	0,02	0,0042	0,0066
5	0,0255	0,0315	0,0705	0,0236	0	0,0315	0,003	0	0,0475	0,0105	0,0255	0,0065	0,0345
7	0,0544	0,009	0,0234	0,0177	0	0,0092	0,0042	0	0,0298	0,0138	0,0486	0,0152	0,0094
9	0,055	0,036	0,063	0,0138	0,044	0,037	0	0	0,086	0	0,054	0,028	0,081
11	0,0766	0,0092	0,0258	0,0096	0,0046	0,011	0,0022	0	0,0168	0,0202	0,0576	0,0196	0,0138
12	0,0762	0	0,017	0,0078	0,0154	0,0122	0,002	0	0	0	0,0692	0,0216	0,008
13	0,0948	0	0,0326	0,0012	0	0,0172	0	0	0,0336	0,0542	0,0394	0,012	0,0144
15	0,1034	0,0072	0,0236	0,0026	0	0,016	0,002	0	0	0,0936	0,0358	0,0132	0,0112
16	0,1161	0	0	0	0	0,0276	0,0087	0	0,0579	0,1785	0,0189	0,0081	0,0234
18	0,099	0,0046	0,0134	0	0	0,011	0,0012	0	0	0,1798	0,0106	0	0,0098
21	0,1284	0,0054	0,022	0,0194	0	0,013	0,004	0,0012	0,0064	0,2366	0,0064	0	0,0146

773 **Supplementary information Table 1:** Evolution of transient compounds (in mM) over the enrichment on Nitrate measured by NMR

774

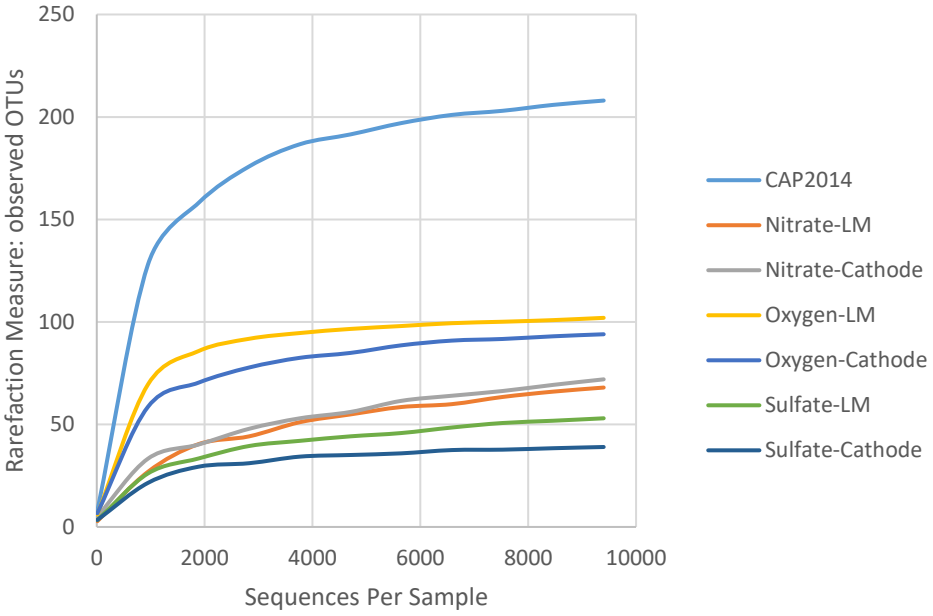


775

776 **Supplementary information Figure S6:** Screening of potentials in abiotic and anaerobic conditions to select the lowest potential before water electrolysis.

777 Potential are expressed vs. SHE.

bioRxiv preprint doi: https://doi.org/10.1101/2020.11.11.377697; this version posted November 11, 2020. The copyright holder for this preprint (which was not certified by peer review) is the author/funder. All rights reserved. No reuse allowed without permission.



778

779 **Supplementary Information Figure S7.** Rarefaction curves of 16S rDNA sequences for bacterial

780 and archaeal diversities in the different samples. Curves were calculated on OTUs at 97%

781 similarity.

782

783